BAF controls cGAS activity on nuclear DNA to prevent innate immune activation

Baptiste Guey[1, §], Marilena Wischnewski[1, §], Alexiane Decout[1], Kristina Makasheva[2], Murat Kaynak[3], Mahmut S. Sakar[3], Beat Fierz[2], Andrea Ablasser[1,]*

[1]Global Health Institute, Swiss Federal Institute of Technology Lausanne (EPFL), Switzerland

[2]Institute of Chemical Sciences and Engineering, Swiss Federal Institute of Technology Lausanne (EPFL), Switzerland

[3]Institute of Mechanical Engineering, Swiss Federal Institute of Technology Lausanne (EPFL), Switzerland

[§] These authors contributed equally to this work.

[*] Correspondence should be addressed to A.A.

One Sentence Summary: BAF competes with cGAS for binding to nuclear self-DNA and, thereby, prevents autoreactivity.

ABSTRACT

The appearance of DNA in the cytosol is perceived as a danger signal that stimulates potent immune responses via cyclic GMP–AMP synthase (cGAS). How cells regulate the activity of cGAS towards self-DNA and guard against potentially damaging autoinflammatory responses is a fundamental biological question. Here we identify barrier-to-autointegration factor 1 (BAF) as a natural opponent of cGAS activity on genomic self-DNA. We show that BAF dynamically outcompetes cGAS for DNA binding hence prohibiting the formation of DNA–cGAS complexes essential for enzymatic activity. Upon loss of nuclear compartmentalization, BAF is necessary to restrict cGAS activity on exposed DNA. Our observations reveal a safeguard mechanism, distinct from physical separation, by which cells protect themselves against aberrant immune responses towards self-DNA. **[120 words]**

36 The enzyme cGAS is a universal innate sensor for double-stranded (ds)DNA *(1, 2)*. On binding dsDNA, cGAS
37 synthesizes the second messenger cyclic GMP–AMP (cGAMP) *(3-7)*. cGAMP, in turn, activates STING to
38 initiate a downstream signaling cascade culminating in the production of type I interferons and other
39 inflammatory mediators (*8*).

40 The physical separation between nuclear DNA and cytoplasmic cGAS by the nuclear envelope (NE)
41 is viewed as a crucial regulatory strategy to avoid aberrant innate immune activation (*9*). However, transient
42 loss of nuclear integrity can occur during normal physiological processes, likely requiring an
43 "immunologically silent" resolution and repair process (*10-12*). At present, it remains unclear how cGAS is
44 controlled during transient openings of the NE.

45 To interrogate cGAS responses towards disrupted nucleo-cytoplasmic compartmentalization, we
46 reduced the levels of key factors known to support NE assembly at the end of mitosis with short interfering
47 RNAs (siRNAs) and monitored levels of interferon-stimulated genes (ISGs) as a surrogate read-out for cGAS
48 activity in HeLa cells *(13)*. We found that downregulation of barrier-to-autointegration factor 1 (*BAF*), encoded
49 by *BANF1*, triggered a robust ISG response, whereas knockdown (KD) of other relevant genes had no effect
50 (Fig. 1A and fig. S1A). The induction of ISGs was completely abrogated in cGAS-deficient cells (Fig. 1A).
51 Furthermore, KD of *BAF* resulted in cGAMP production and activation of TBK1 (Fig. 1, B and C). Similar
52 results were obtained in mouse embryonic fibroblasts and human fibroblasts (fig. S1, B to F). Thus, BAF
53 appears to exert an important regulatory function over cGAS, defects of which trigger innate immune
54 activation.

55 BAF is essential for nuclear membrane reformation at the end of mitosis *(13-16)*. However, arresting
56 *BAF*-KD cells in S phase of the cell cycle had no effect on the induced ISG response (fig. S2A). Moreover,
57 ISG upregulation was not accompanied by a detectable increase in micronuclei or by the appearance of
58 cytosolic chromatin fragments (fig. S2, B to E). Instead, *BAF*-KD cells showed repetitive NE rupture events,
59 which were strongly correlated with the accumulation of cGAS within discrete intranuclear foci (Fig. 1, D to
60 F and fig. S3, A to D). Live-cell imaging confirmed that cGAS was recruited towards the nucleus interior
61 following loss of NE integrity (Fig. 1G and movie S1). Stabilizing the NE with the myosin II inhibitor
62 blebbistatin not only prevented NE ruptures after *BAF* KD, but also completely abrogated cGAS activity (Fig.
63 1H and fig. S3E). Interestingly, disrupting NE integrity through altering the nuclear lamina via KD of *LMNA*,
64 encoding for lamin A, or through mechanical compression did not induce an ISG response, despite cGAS

65 nuclear translocation (Fig. 2, A and B, fig. S4, and fig. S5) *(17-19)*. However, mechanically induced NE
66 breakdown in *BAF*-KD cells elicited cGAS–STING pathway activation, as revealed by robust IRF3 activation
67 (Fig. 2, C and D). Thus, these data indicate that the control of cGAS activity against nuclear self-DNA depends
68 on more than just the nuclear membrane and implicate a key regulatory function for BAF.

69 To explore the mechanism by which BAF restricts cGAS activity, we considered BAF's functional
70 properties to bind dsDNA and to interact with inner nuclear membrane proteins via the LEM
71 (Lap2/Emerin/Man1)-domain (*16*). Whereas reconstitution of *BAF*-KD cells with a mutant defective in LEM-
72 domain binding, *BAF L58R (16)*, or the combined depletion of LEM-domain proteins had no effect,
73 reconstitution with a *BAF* mutant compromised in DNA binding, *BAF G47E (20),* induced ISG upregulation
74 (Fig. 3A and fig. S6, A-D). We therefore considered that BAF may prevent cGAS activity by competing for
75 DNA binding. Using purified components, we determined that wild-type (WT) BAF, but not BAF G47E, dose-
76 dependently reduced cGAS binding to chromatin and dsDNA, respectively (Fig. 3B and fig. S6, E and F).
77 Moreover, BAF robustly inhibited DNA-dependent cGAMP synthesis in vitro, whereas BAF G47E had no
78 such effect (Fig. 3, C and D). We next used single-molecule total internal reflection fluorescence (smTIRF)
79 microscopy to visualize in real-time the binding of individual cGAS molecules to dsDNA (fig. S7, A to C).
80 Single-molecule traces revealed that cGAS engaged in very transient ($\tau_{off,1}$ = 1.4 ± 0.5 s) and occasionally
81 longer ($\tau_{off,2}$ = 15 ± 5 s) interactions with dsDNA (Fig. 3, E and H, and fig. S7D). When BAF was added, there
82 was no change in the binding rate (k_{on}) of cGAS on dsDNA. Instead, BAF WT, but not BAF G47E, led to the
83 rapid dissociation of cGAS from dsDNA, as indicated by a marked (3-5-fold) reduction of the average dwell
84 times ($\tau_{off,1}$, $\tau_{off,2}$) (Fig. 3, F-H, and fig. S7D). Thus, rather than passively interfering with cGAS activity by
85 blocking DNA binding sites, BAF dynamically displaces transiently bound cGAS monomers from dsDNA.

86 The above data suggest a model where BAF outcompetes cGAS on DNA, thereby preventing the
87 formation of oligomeric DNA–cGAS assemblies, which is required for enzymatic activity (*21*). Under this
88 model, cGAS should form larger and more stable complexes with DNA exposed at the site of NE rupture if
89 BAF was absent. Monitoring cGAS intracellular localization at a given moment in time revealed that a large
90 fraction of *BAF*-KD cells accumulated cGAS in the nucleus (Fig. 4A). By contrast, only few *LMNA*-KD cells
91 showed intranuclear cGAS accumulation (Fig. 4A). In addition, for those nuclei that accumulated cGAS, the
92 intranuclear volume covered by cGAS was significantly larger when *BAF* was downregulated (Fig. 4, A (inset),
93 B and C). Using fluorescence recovery after photobleaching (FRAP), we also found that cGAS was less mobile

94 on chromatin in *BAF*-KD versus *LMNA*-KD cells or control cells, respectively (Fig. 4D, fig. S8, A, B and C,
95 and movie S2). Critically, the frequency of rupture events as well as the overall rate of NE repair was similar
96 under both these conditions (fig. S8D). Thus, in living cells BAF limits cGAS associations with chromatin
97 after NE rupture, consistent with the competition for DNA binding.

98 BAF has been implicated in the recognition of exogenous dsDNA in the cytosol (*22*). Visualizing the
99 recruitment of BAF and cGAS to transfected DNA, revealed a negative correlation between DNA foci that
100 were targeted by cGAS versus BAF and overexpression of BAF enhanced this effect (fig. S9A). We also
101 measured cGAMP production and ISG transcripts and found that overexpression of *BAF* resulted in, at least
102 partially, compromised cGAS activation (fig. S9B). Competition for DNA binding between cGAS and BAF
103 can therefore also occur in the cytosol, albeit with lower overall efficacy.

104 Although the activation of cGAS by DNA typically occurs within the cytosol, a considerable fraction
105 of cGAS resides within the nucleus at steady state (*19, 23*). However, the nuclear pool of cGAS appears
106 functionally inactive through strong binding to chromatin and is considered to not participate in DNA sensing
107 and activation (*23, 24*). To understand the relationship between the inhibitory effect of chromatin versus BAF
108 for cGAS regulation, we used two distinct *CGAS* mutants, *CGAS R236A* and *R255A*, defective in nuclear
109 tethering (*23*). Consistent with prior work (*23*), cells expressing either mutant showed spontaneous cGAMP
110 synthesis, presumably as a result of nuclear DNA sensing. KD of *BAF* markedly enhanced the overall level of
111 cGAMP production from both *CGAS*-mutant cells, whereas overexpression of *BAF* reduced cGAMP synthesis
112 (fig. S10, A and B). We also generated cells that selectively express cGAS inside the nucleus (*GFP-NLS-*
113 *CGAS*) to lower the threshold of intranuclear cGAS activation. KD of *BAF* in this experimental system led to
114 prominent cGAS activity even in the absence of NE ruptures (Fig. 4E). Finally, we investigated whether other
115 chromatin organizing factors exert similar regulatory function over cGAS (*25*). Using the cGAS–NLS
116 experimental system, we found that compared to several other architectural chromatin proteins KD of *BAF*
117 had by far the strongest effect on both cGAMP production as well as ISG upregulation (fig. S11, A, B and C).
118 Moreover, decondensing chromatin by treating cells with the histone deacetylase inhibitors valproic acid (VA)
119 and trichostatin A (TSA) did not trigger NLS–cGAS activity and neither did overexpressing *HMGN5* in HeLa
120 cells (fig. S11, D and E) (*26*). Thus, although the precise role of chromatin architecture and chromatin itself
121 requires further study, our experimental findings provide strong evidence that BAF acts as a critical regulatory
122 factor over cGAS on nuclear DNA.

123 This study identifies a safeguard mechanism that restricts cGAS activity on genomic self-DNA: Upon
124 loss of nuclear compartmentalization, cytosolic cGAS accumulates on chromatin at the nuclear periphery, but
125 its enzymatic activity is prevented by BAF, which dynamically outcompetes cGAS for DNA binding. Although
126 limiting cGAS activity against self-DNA depends on compartmentalization in certain situations (e.g.,
127 mitochondria, micronuclei, and cytosolic chromatin fragments) *(2, 9)*, our work implicates that regulation of
128 nuclear DNA sensing requires more complex mechanisms than simple physical separation. We propose that
129 dynamic competition with BAF at the nuclear periphery is a critical strategy used by the host to reconcile the
130 advantages of maintaining a universal DNA recognition machinery with routine operations occurring within a
131 living cell.
132

133 **REFERENCES AND NOTES**

134 1. L. Sun, J. Wu, F. Du, X. Chen, Z. J. Chen, Cyclic GMP-AMP synthase is a cytosolic DNA sensor that
135 activates the type I interferon pathway. *Science* **339**, 786-791 (2013).
136 2. A. Ablasser, Z. J. Chen, cGAS in action: Expanding roles in immunity and inflammation. *Science* **363**,
137 (2019).
138 3. A. Ablasser *et al.*, cGAS produces a 2'-5'-linked cyclic dinucleotide second messenger that activates
139 STING. *Nature* **498**, 380-384 (2013).
140 4. E. J. Diner *et al.*, The innate immune DNA sensor cGAS produces a noncanonical cyclic dinucleotide
141 that activates human STING. *Cell Rep* **3**, 1355-1361 (2013).
142 5. P. Gao *et al.*, Cyclic [G(2',5')pA(3',5')p] is the metazoan second messenger produced by DNA-
143 activated cyclic GMP-AMP synthase. *Cell* **153**, 1094-1107 (2013).
144 6. J. Wu *et al.*, Cyclic GMP-AMP is an endogenous second messenger in innate immune signaling by
145 cytosolic DNA. *Science* **339**, 826-830 (2013).
146 7. X. Zhang *et al.*, Cyclic GMP-AMP containing mixed phosphodiester linkages is an endogenous high-
147 affinity ligand for STING. *Mol Cell* **51**, 226-235 (2013).
148 8. G. N. Barber, STING: infection, inflammation and cancer. *Nat Rev Immunol* **15**, 760-770 (2015).
149 9. A. Ablasser, S. Hur, Regulation of cGAS- and RLR-mediated immunity to nucleic acids. *Nat Immunol*
150 **21**, 17-29 (2020).

151 10. C. M. Denais *et al.*, Nuclear envelope rupture and repair during cancer cell migration. *Science* **352**,
152 353-358 (2016).
153 11. M. Raab *et al.*, ESCRT III repairs nuclear envelope ruptures during cell migration to limit DNA
154 damage and cell death. *Science* **352**, 359-362 (2016).
155 12. R. Ungricht, U. Kutay, Mechanisms and functions of nuclear envelope remodelling. *Nat Rev Mol Cell*
156 *Biol* **18**, 229-245 (2017).
157 13. T. Haraguchi *et al.*, Live cell imaging and electron microscopy reveal dynamic processes of BAF-
158 directed nuclear envelope assembly. *J Cell Sci* **121**, 2540-2554 (2008).
159 14. T. Haraguchi *et al.*, BAF is required for emerin assembly into the reforming nuclear envelope. *J Cell*
160 *Sci* **114**, 4575-4585 (2001).
161 15. A. Margalit, M. Segura-Totten, Y. Gruenbaum, K. L. Wilson, Barrier-to-autointegration factor is
162 required to segregate and enclose chromosomes within the nuclear envelope and assemble the nuclear
163 lamina. *Proc Natl Acad Sci U S A* **102**, 3290-3295 (2005).
164 16. M. Samwer *et al.*, DNA Cross-Bridging Shapes a Single Nucleus from a Set of Mitotic Chromosomes.
165 *Cell* **170**, 956-972 e923 (2017).
166 17. W. H. De Vos *et al.*, Repetitive disruptions of the nuclear envelope invoke temporary loss of cellular
167 compartmentalization in laminopathies. *Hum Mol Genet* **20**, 4175-4186 (2011).
168 18. M. Le Berre, E. Zlotek-Zlotkiewicz, D. Bonazzi, F. Lautenschlaeger, M. Piel, Methods for two-
169 dimensional cell confinement. *Methods Cell Biol* **121**, 213-229 (2014).
170 19. M. Gentili *et al.*, The N-Terminal Domain of cGAS Determines Preferential Association with
171 Centromeric DNA and Innate Immune Activation in the Nucleus. *Cell Rep* **26**, 3798 (2019).
172 20. T. C. Umland, S. Q. Wei, R. Craigie, D. R. Davies, Structural basis of DNA bridging by barrier-to-
173 autointegration factor. *Biochemistry* **39**, 9130-9138 (2000).
174 21. L. Andreeva *et al.*, cGAS senses long and HMGB/TFAM-bound U-turn DNA by forming protein-
175 DNA ladders. *Nature* **549**, 394-398 (2017).
176 22. S. Kobayashi *et al.*, BAF is a cytosolic DNA sensor that leads to exogenous DNA avoiding autophagy.
177 *Proc Natl Acad Sci U S A* **112**, 7027-7032 (2015).
178 23. H. E. Volkman, S. Cambier, E. E. Gray, D. B. Stetson, Tight nuclear tethering of cGAS is essential
179 for preventing autoreactivity. *Elife* **8**, (2019).

180 24. C. Zierhut *et al*., The Cytoplasmic DNA Sensor cGAS Promotes Mitotic Cell Death. *Cell* **178**, 302-
181 315 e323 (2019).
182 25. S. J. McBryant, V. H. Adams, J. C. Hansen, Chromatin architectural proteins. *Chromosome Res* **14**,
183 39-51 (2006).
184 26. T. Furusawa *et al*., Chromatin decompaction by the nucleosomal binding protein HMGN5 impairs
185 nuclear sturdiness. *Nat Commun* **6**, 6138 (2015).
186 27. P. T. Lowary, J. Widom, New DNA sequence rules for high affinity binding to histone octamer and
187 sequence-directed nucleosome positioning. *J Mol Biol* **276**, 19-42 (1998).
188 28. T. Aggarwal, D. Materassi, R. Davison, T. Hays, M. Salapaka, Detection of Steps in Single Molecule
189 Data. *Cell Mol Bioeng* **5**, 14-31 (2012).
190 29. S. Kilic *et al*., Single-molecule FRET reveals multiscale chromatin dynamics modulated by HP1alpha.
191 *Nat Commun* **9**, 235 (2018).
192

193 **ACKNOWLEDGEMENTS**

194 We thank N. Jordan and J. Ricci for technical assistance. We thank T. Laroche, R. Guiet, O. Burri, and A.
195 Seitz of the Bioimaging and optics platform (BIOP) at EPFL. **Funding:** A.A. is supported by the SNF
196 (BSSGI0-155984, 31003A_159836), the Gebert Rüf Foundation (GRS-059_14), the NCCR Chemical
197 Biology, and the ERC (804933, ImAgine). B.G. has been awarded a Long-term EMBO fellowship. B.F. is
198 supported by the ERC (724022, chromo-SUMMIT) and the NCCR in Chemical Biology. M.S.S. is supported
199 by the ERC (714609, ROBOCHIP). **Author contributions:** B.G. and A.A. designed the study. B.G., M.W.,
200 A.D., K.M., and M.K., performed experiments, all authors analyzed the data. A.A. wrote the manuscript with
201 input from all authors and supervised the study. **Competing interests:** A.A. is member of the scientific
202 advisory board of IFM Therapeutics and scientific co-founder of IFM Due. All other authors declare no conflict
203 of interest. **Data and materials availability:** All data are available in the main text or the supplementary
204 materials.
205

206 **Supplementary Materials:**

207 Materials and Methods

208 Figures S1-S11

209 Movies S1-S2

210 References (*27-29*)

211

212 **Fig. 1. BAF depletion causes nuclear envelope rupture and cGAS activation on chromatin.** (**A**) ISG
213 (*ISG15*, *IFI44*) induction in WT and *CGAS*$^{-/-}$ HeLa cells treated with a control siRNA (siCtrl) or siRNAs
214 against *BAF* (siBAF.1, siBAF.2) (N = 6). One-way ANOVA with post hoc Tukey multiple comparison test.
215 (**B**) 2'3'-cGAMP quantification in HeLa cells treated with siCtrl, siBAF, or transfected with 90mer dsDNA
216 (dsDNA) (N = 6). One-way ANOVA with post hoc Dunnett multiple comparison test. (**C**) Phosphorylation of
217 TBK1 in HeLa cells after *BAF* knockdown. (**D**) Confocal fluorescence microscopy images of *BAF*-KD HeLa
218 cells stained with antibodies against cGAS (green) and lamin A (red). DAPI shown in blue. Scale bar: 20 μm
219 or 5 μm (Zoom). (**E**) Left: Fluorescence microscopy images showing a NE rupture event (NLS-GFP escape
220 (green)). Right: Incidence of NE ruptures in HeLa cells upon treatment with a control siRNA or one targeting
221 *BAF*. See also complete image sequence in fig. S3B. Scale bar: 20 μm. (N = 3). Student's t test. (**F**) NLS-GFP
222 fluorescence ratio cytosol/nucleus in *BAF*-depleted HeLa cells exhibiting or not cGAS nuclear foci. Student's
223 t test. (**G**) Representative image sequence of a *BAF*-depleted HeLa cell exhibiting a NE rupture event (NLS-
224 GFP (green) escape) accompanied by cGAS-Halo (orange) intranuclear accumulation. See also movie S1.
225 Asterisk marks cGAS in a micronucleus. Scale bar: 20 μm or 5 μm (Zoom). (**H**) 2'3'-cGAMP quantification in
226 HeLa cells pre-treated or not with blebbistatin and treated siCtrl, siBAF, or transfected with 90mer DNA
227 (dsDNA) (N = 5). One-way ANOVA with post hoc Dunnett multiple comparison test. Error bars, SEM. *P <
228 0.05; **P < 0.01; ***P < 0.001; ****P < 0.0001; ns, not significant.

229

230 **Fig. 2. Loss of nuclear integrity is not uniformly linked to cGAS activity.** (**A**) Incidence of NE ruptures in
231 HeLa cells treated with siCtrl, siBAF, or siLMNA (N = 3). Multiple t test. (**B**) *ISG15* mRNA expression levels
232 in HeLa cells treated with siCtrl, siBAF, or siLMNA. (N = 6). One-way ANOVA with post hoc Dunnett
233 multiple comparison test. (**C**) Quantification of cells with cGAS-positive nuclei showing GFP-IRF3 nuclear
234 translocation after confinement of HeLa treated with blebbistatin (20 μM) and siCtrl or siBAF, respectively
235 (N = 4). Student's t test. (**D**) Representative image of HeLa cells stably expressing GFP-IRF3 (green) and

236 cGAS-Halo (red), treated with blebbistatin (20 μM), siCtrl or siBAF, and subjected to 3-μm confinement for
237 1 min. Image was acquired 5 hours after confinement. Scale bar: 40 μm. Error bars, SEM. *$P < 0.05$; **$P <$
238 0.01; ****$P < 0.0001$; ns, not significant.

239

240 **Fig. 3. Molecular mechanism of cGAS inhibition by BAF.** (**A**) *ISG15* mRNA expression levels of HeLa
241 cells (Ctrl) and siRNA-resistant *BAF (WT)* and *BAF G47E* expressing HeLa cells depleted or not for *BAF* (N
242 = 5). One-way ANOVA with post hoc Dunnett multiple comparison test. (**B**) Labeled-cGAS intensity obtained
243 via confocal microscopy of chromatin particles pre-incubated or not with BAF ($N = 3$). One-way ANOVA
244 with post hoc Dunnett multiple comparison test. (**C**) In vitro analysis of 2'3'-cGAMP synthesis by dsDNA-
245 stimulated cGAS and addition of BAF (WT) or G47E. (**D**) Ratio of in vitro 2'3'-cGAMP synthesis between
246 cGAS stimulated with dsDNA pre-complexed with BAF (WT) or BAF G47E, and free dsDNA, ($N = 3$),
247 multiple *t* test. (**E** to **G**) Extracted single-molecule (sm) fluorescence time trace (left) and corresponding dwell-
248 time histograms for cGAS in the absence of BAF (E), cGAS in the presence of BAF (WT) (F), and cGAS in
249 the presence of BAF G47E (G), showing stochastic binding events. (**H**) Dwell times ($\tau_{off,1}$; $\tau_{off,2}$) for cGAS,
250 cGAS + BAF (WT), cGAS + BAF G47E. (N = 4 (cGAS), N = 3 (cGAS + BAF WT), N = 4 (cGAS + BAF
251 G47E) [independent experiments]). Two-tailed Student's *t* test. Error bars, SEM. *$P < 0.05$; **$P < 0.01$; ***P
252 < 0.001; ****$P < 0.0001$; ns, not significant.

253

254 **Fig. 4. BAF outcompetes cGAS from DNA in living cells.** (**A**) Left: Fluorescence microscopy images of
255 HeLa cells treated with a siCtrl, siBAF, or siLMNA for 3 days and stained for cGAS (green) and DNA
256 (DRAQ5, red). Scale bar: 20 μm. Right top: quantification of nuclei exhibiting cGAS nuclear foci for each
257 condition as indicated (N = 3). One-way ANOVA with post hoc Dunnett multiple comparison test. Right
258 bottom: Enlargement of indicated nuclei. (**B** and **C**) High-resolution confocal fluorescence microscopy images
259 of cGAS nuclear foci and measurement of cGAS nuclear volume in HeLa cells treated for 3 days with siBAF
260 or siLMNA. Cells were stained for cGAS (green) and DNA (DRAQ5, red). Scale bar: 5 μm (representative of
261 three independent experiments). (**D**) cGAS-GFP immobile fraction obtained after photobleaching of cGAS-
262 GFP nuclear foci in HeLa cells treated with siCtrl, siBAF, or siLMNA (representative of three independent
263 experiments). One-way ANOVA with post hoc Dunnett multiple comparison test. (**E**) 2'3'-cGAMP levels from
264 WT HeLa, *CGAS*$^{-/-}$ HeLa or *CGAS*$^{-/-}$ HeLa cells overexpressing NLS-cGAS (*GFP-NLS-CGAS*) and treated

265 with siCtrl, siBAF, or transfected with 90mer DNA (dsDNA). The graph shows means of independent
266 experiments ($N = 5$). Two-way ANOVA with post hoc Dunnett multiple comparison test. Error bars, SEM. *P
267 < 0.05; **$P < 0.01$; ***$P < 0.001$; ns, not significant.

Figure 1

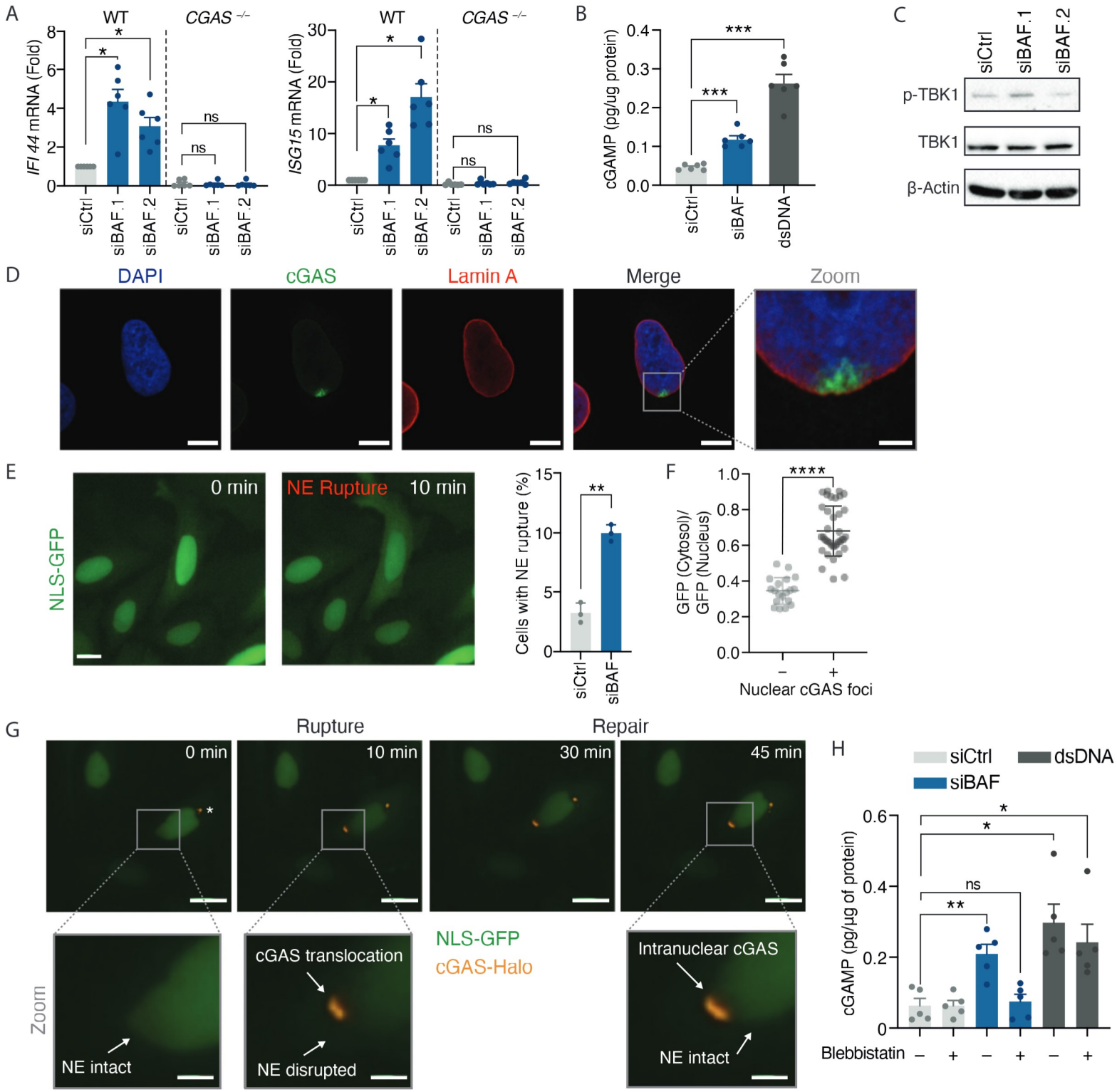
A
WT
CGAS -/-
IFI 44 mRNA (Fold)
ISG15 mRNA (Fold)
siCtrl
siBAF.1
siBAF.2
ns
B
cGAMP (pg/ug protein)
siBAF
dsDNA
C
p-TBK1
TBK1
β-Actin
D
DAPI
cGAS
Lamin A
Merge
Zoom
E
NLS-GFP
0 min
NE Rupture
10 min
Cells with NE rupture (%)
F
GFP (Cytosol)/ GFP (Nucleus)
Nuclear cGAS foci
G
Rupture
Repair
30 min
45 min
Zoom
NE intact
cGAS translocation
NE disrupted
NLS-GFP
cGAS-Halo
Intranuclear cGAS
H
siCtrl
siBAF
dsDNA
cGAMP (pg/µg of protein)
Blebbistatin

Figure 2

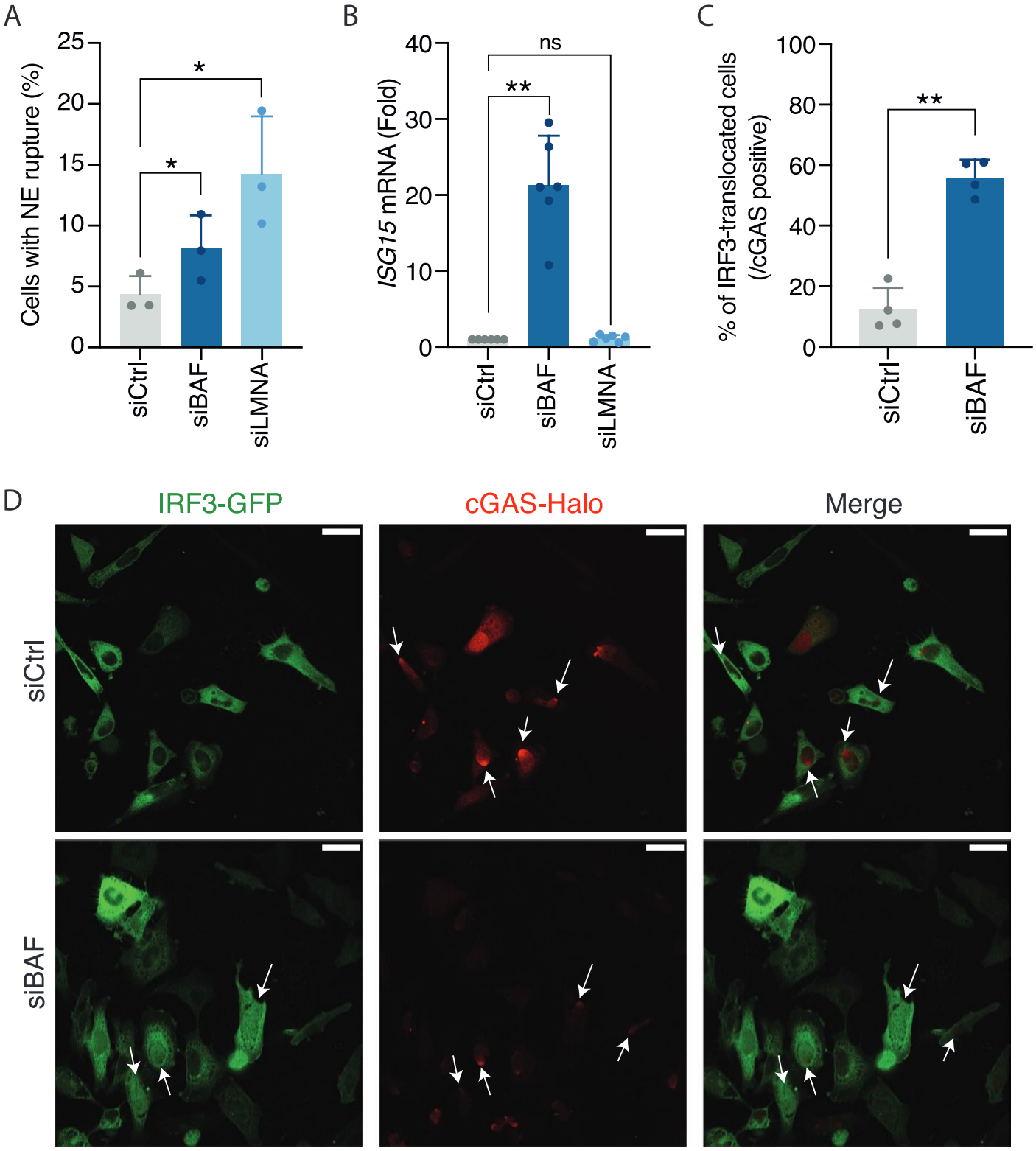
A
Cells with NE rupture (%)
25
20
15
10
5
0
*
*
siCtrl
siBAF
siLMNA
B
ISG15 mRNA (Fold)
40
30
20
10
0
ns
**
siCtrl
siBAF
siLMNA
C
% of IRF3-translocated cells (/cGAS positive)
100
80
60
40
20
0
**
siCtrl
siBAF
D
IRF3-GFP
cGAS-Halo
Merge
siCtrl
siBAF

Figure 3

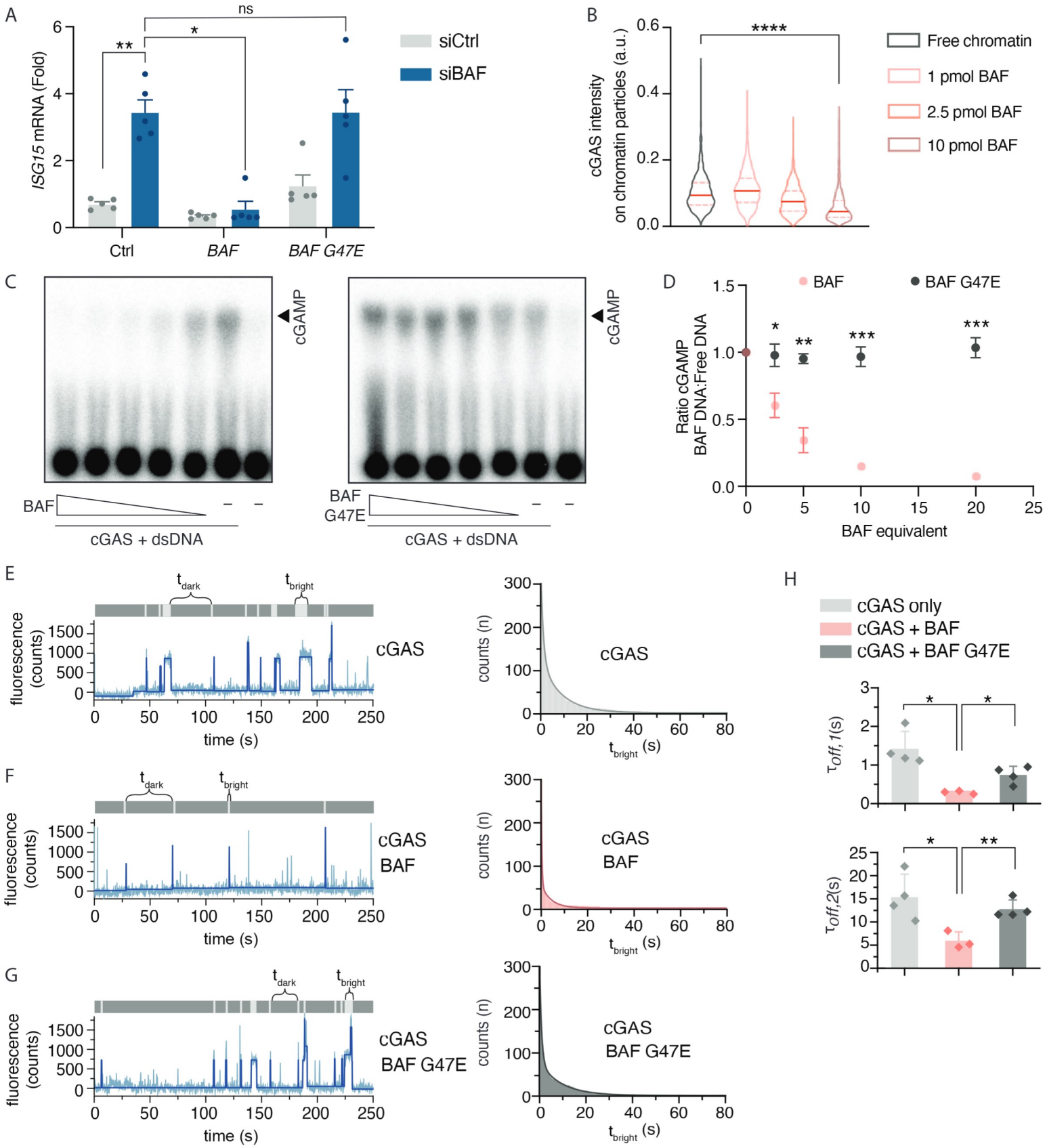
A
ISG15 mRNA (Fold)
ns
*
**
siCtrl
siBAF
Ctrl
BAF
BAF G47E
B
cGAS intensity on chromatin particles (a.u.)
****
Free chromatin
1 pmol BAF
2.5 pmol BAF
10 pmol BAF
C
cGAMP
BAF
BAF G47E
cGAS + dsDNA
D
BAF
BAF G47E
Ratio cGAMP BAF DNA:Free DNA
BAF equivalent
E
F
G
fluorescence (counts)
time (s)
cGAS
cGAS BAF
cGAS BAF G47E
counts (n)
H
cGAS only
cGAS + BAF
cGAS + BAF G47E
τoff,1(s)
τoff,2(s)

Figure 4

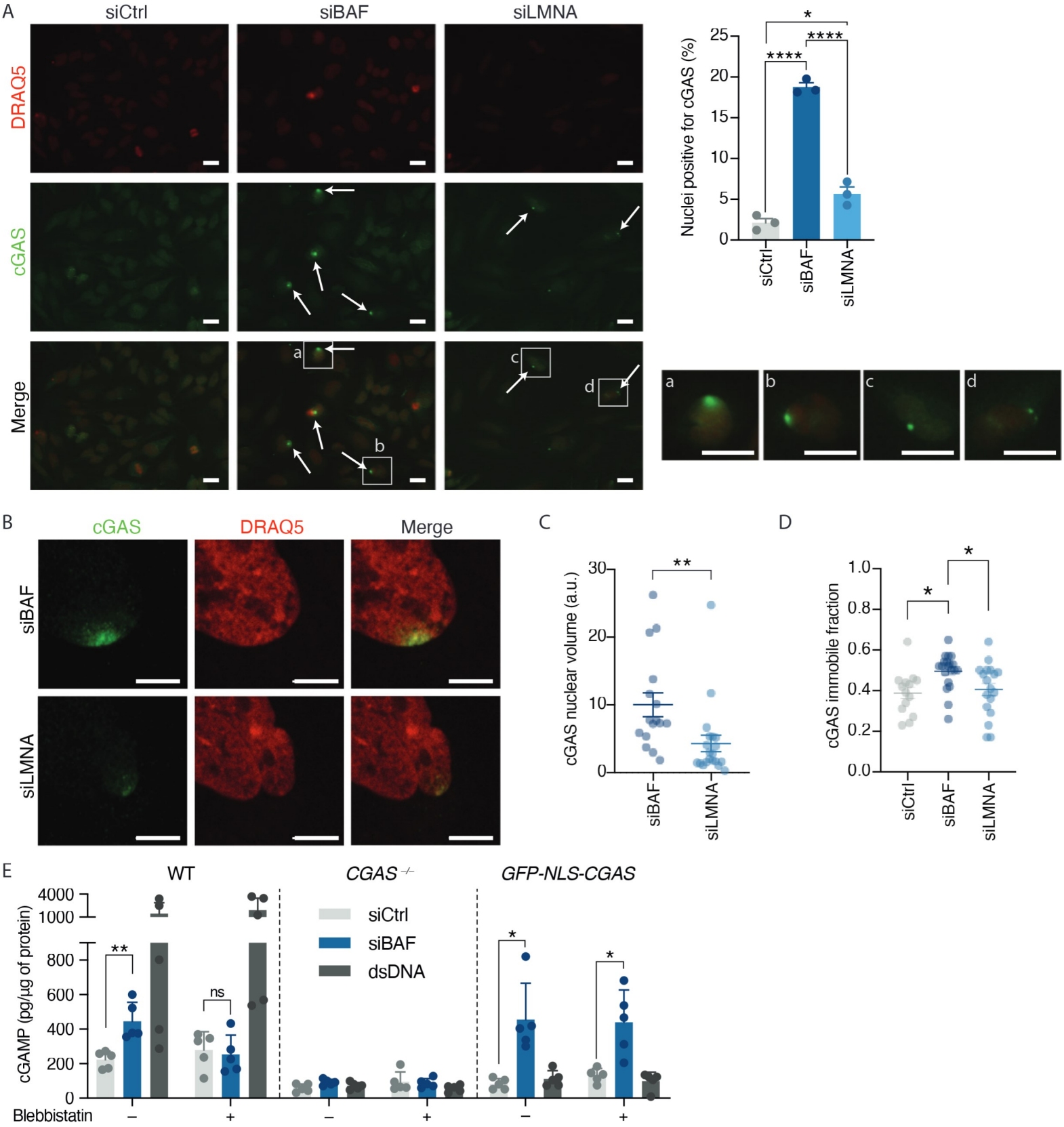
A
siCtrl
siBAF
siLMNA
DRAQ5
cGAS
Merge
a
b
c
d
Nuclei positive for cGAS (%)
25
20
15
10
5
0
*
****
****
siCtrl
siBAF
siLMNA
B
cGAS
DRAQ5
Merge
siBAF
siLMNA
C
cGAS nuclear volume (a.u.)
30
20
10
0
**
siBAF
siLMNA
D
cGAS immobile fraction
1.0
0.8
0.6
0.4
0.2
0.0
*
*
siCtrl
siBAF
siLMNA
E
WT
CGAS -/-
GFP-NLS-CGAS
cGAMP (pg/µg of protein)
4000
1000
800
600
400
200
0
**
ns
*
*
siCtrl
siBAF
dsDNA
Blebbistatin
–
+
–
+
–
+

Supplementary Materials for

BAF controls cGAS activity on nuclear DNA to prevent innate immune activation

Baptiste Guey[1, §], Marilena Wischnewski[1, §], Alexiane Decout[1], Kristina Makasheva[2], Murat Kaynak[3], Mahmut S. Sakar[3], Beat Fierz[2], Andrea Ablasser[1,*]

correspondence to: andrea.ablasser@epfl.ch (A.A.)

This PDF file includes:

Materials and Methods
Figs. S1 to S11
Captions for Movies S1 to S2

Other Supplementary Materials for this manuscript includes the following:

Movies S1 to S2

Materials and Methods

Cell culture and generation of specific cell lines

To establish HeLa *NLS-GFP*, HeLa *eGFP-IRF3*, HeLa *CGAS-GFP* and HeLa *HMGN5* cells, HeLa wild-type (WT) cells were infected with a pTRIPZ lentiviral vector carrying *NLS-GFP*, *eGFP-IRF3*, *CGAS-GFP*, or *HMGN5*, respectively, and a puromycin-resistance gene. Cells were selected with puromycin (1 µg/ml). To establish HeLa *NLS-GFP* or *eGFP-IRF3* cells co-expressing *CGAS-K231K-Halo*, cells were infected with a pRRL lentiviral vector (kind gift from D. Trono) carrying *CGAS-K231K-Halo* and a blasticidin-resistance gene. Cells were selected using blasticidin (5 µg/ml). To establish HeLa NLS-cGAS cells, HeLa *CGAS*$^{-/-}$ cells were infected with a pTRIPZ lentiviral vector carrying *GFP-NLS-CGAS* and a puromycin resistance gene. Cells were selected using puromycin (1 µg/ml). To establish HeLa *CGAS* (WT), HeLa *CGAS R255A* and HeLa *CGAS R236A* cells, HeLa *CGAS*$^{-/-}$ cells were infected with a pTRIPZ lentiviral vector carrying *CGAS WT-FLAG*, *CGAS R255A-FLAG* or *CGAS R236A-FLAG*, respectively, and a puromycin-resistance gene. Cells were selected with puromycin (1 µg/ml). To establish distinct BAF mutant HeLa cell lines, we cloned human *BAF (BANF1)* into a pDNR plasmid and used mutagenesis PCR to introduce respective mutation within the *BAF* gene (c.140GC>AG for p.G47E and c.173T>G for p.L58R). Each mutated gene was cloned into a pTRIPZ vector for lentivirus production. HeLa cells were infected with the pTRIPZ lentiviral vector carrying the WT or respective mutated *BAF* and a puromycin-resistance gene. Cells were selected with puromycin (1 µg/ml). To induce overexpression of the lentiviral vector-encoded genes, cells were treated with 1 µg/ml of doxycycline.

HeLa and WI-38 cells were cultured in DMEM medium (Thermo Fisher Scientific, 41965039) supplemented with 10% (v/v) heat-inactivated FBS (Thermo Fisher Scientific, Gibco SKU, 10270106), 100 IU/ml penicillin/streptomycin (BioConcept, 4-01F00-H), 2 mM L-glutamine (Thermo Fisher Scientific, 25030024). MEFs were cultured in DMEM supplemented with 15% (v/v) heat-inactivated FBS (Thermo Fisher Scientific, Gibco SKU, 10270106) and 100 IU/ml penicillin/streptomycin (BioConcept, 4-01F00-H). Primary human adult dermal fibroblasts and primary human neonatal foreskin fibroblasts were cultured in DMEM supplemented with 15% (v/v) heat-inactivated FBS (Thermo Fisher Scientific, Gibco SKU, 10270106), 2 mM L-glutamine (Thermo Fisher Scientific, 25030024), 100 IU/ml penicillin/streptomycin (BioConcept, 4-01F00-H) and 1% non-essential amino acids (Thermo Fisher Scientific, Gibco, 11140035). HeLa, WI-38, MEFs and primary cells were cultivated at 37°C and 5% CO_2.

Transfections

Cells were transfected with siRNAs using Lipofectamine®RNAimax reagent (Thermo Fisher Scientific) according to the manufacturer's instructions. Silencer select predesigned siRNAs were purchased from Thermo Fisher Scientific: Negative Control (Cat.No. 4390847); siRNA directed against human targets: siBAF: siBANF1_1 ID: s16807, siBANF1_2 ID:46065, siBANF1_3 ID: s16808; siLMNA_1 ID: s8221, siLMNA_2 ID: s8222, siEMD_1 ID: s4645, siEMD_2 ID: s4647, siTMPO_1 ID: s14233, siTMPO_2 ID: s14234, siLEMD3_1 ID: s527438, siLEMD3_2 ID: s527439, siMECP2_1 ID: s8644, siMECP2_2 ID: s8646, siHIST1H1E_1 ID: s6402,

siHIST1H1D_1 ID: s6398, siHIST1H1C_1 ID: s194486, siHIST1H1E_2 ID: s226269, siHIST1H1D_2 ID: s6400, siHIST1H1C_2 ID: s194487, siEZH1_1 ID: s4913, siEZH1_2 ID: s4914, siCBX5_1 ID: s23884, siCBX5_2 ID: s23885, siSLBP_1 ID: s15448, siSLBP_2 ID: s15449, siCHAF1A_1 ID: s19499, siCHAF1A_2 ID: s19501, siCHAF1B_1 ID: s15704, siCHAF1B_2 ID: s15706, siLBR_1 ID: s8101, siLBR_2 ID: s8102. siRNA directed against mouse targets: siBanf1_1 ID: s76486, siBanf1_2 ID: s203585, siLmna_1 ID: s69252, siLmna_2 ID: s69253. siRNAs were used at a concentration of 20 μM per reaction for HeLa cells, MEFs, and primary human fibroblasts, and at 1.25 μM for WI-38 cells. For combined silencing of LEM-domain containing proteins, or combined silencing of histone H1 cluster, three individual siRNAs, each at a concentration of 10 μM, were combined per reaction ("triple" silencing).

For cGAS activation, cells were transfected with 90mer dsDNA using Lipofectamine®2000 reagent (Thermo Fisher Scientific, 11668019). Briefly, cells were seeded into six-well plates to about 80% confluency. Lipofectamine®2000 reagent (3.5 μl) in 125 μl Opti-MEM (Thermo Fisher Scientific, 31985047) per transfection was incubated with up to 3000 ng 90mer dsDNA per reaction in 125 μl Opti-MEM for 5 min at room temperature before the addition of the mix (240 μl) to the cells.

For transfection with plasmid DNA (pEFBos vector, ~6 kb), cells were transfected using GeneJuice® transfection reagent (Merck Millipore, 70967-6). Briefly, cells were seeded into six-well plates to about 80% confluency. GeneJuice® reagent (3 μl) in 100 μl Opti-MEM (Thermo Fisher Scientific, 31985047) per transfection were incubated with 500 ng of plasmid DNA per reaction in 100 μl Opti-MEM for 15 min at room temperature before the addition of the mix (180 μl) to the cells. For all dsDNA transfections, cells were collected 4 hours after transfection for analysis by qRT-PCR or 2'3'-cGAMP ELISA.

For transient overexpression experiments, cells were transfected with pEFBos vectors (~6 kb) carrying *eGFP* (Ctrl), *BAF WT* or *BAF G47E* using GeneJuice® transfection reagent (Merck Millipore - 70967-6). Briefly, cells were seeded into six-well plates to about 80% confluency. GeneJuice® reagent (3 μl) in 100 μl Opti-MEM (Thermo Fisher Scientific, 31985047) per transfection were incubated with 1000 ng of plasmid DNA per reaction in 100 μl Opti-MEM for 15 min at room temperature before the addition of the mix (180 μl) to the cells. *cGAS* expression was induced 24 hours after transfection by addition of doxycycline (1 μg/ml). Cells were collected 3 days after transfection for analysis by 2'3'-cGAMP ELISA.

Quantitative real-time PCR (RT-qPCR)

Cells were lysed using RLT buffer (Qiagen, 79216). RNA was extracted according to the manufacturer's protocol (Qiagen RNeasy Mini kit) and treated with RNase-free DNase (Thermo Fisher Scientific, EN0521). RNA (500 ng) was reverse transcribed (RevertAid, Thermo Fisher Scientific, EP0442) and analyzed by RT-qPCR in duplicates or triplicates using the Maxima SYBR Green/ROX qPCR Master Mix (Thermo Fisher Scientific, K0223). The qPCR reactions were run on a QuantStudio 5 Real-Time PCR system. GAPDH was used for normalization.

Primer sequences for RT-qPCR:
hs ISG15 forward 5'-CAG CCA TGG GCT GGG AC-3';
hs ISG15 reverse 5'-GCC GAT CTT CTG GGT GAT CT-3';
mm Isg15 forward 5'-AAG AAG CAG ATT GCC CAG AA-3';
mm Isg15 reverse 5'-TCT GCG TCA GAA AGA CCT CA-3';
hs IFI44 forward 5'-GAT GTG AGC CTG TGA GGT CC-3';
hs IFI44 reverse 5'-CTT TAC AGG GTC CAG CTC CC-3';
mm Ifi44 forward 5'-TGC ACT CTT CTG AGC TGG TG-3';
mm Ifi44 reverse 5'-CCA GCT TGG ACT TCA CAG GA-3';
hs BANF1 forward 5'-AGG AAA GGG GTT TTG ACA AGG CC-3';
hs BANF1 reverse 5'-CGA AGG CAT CCG AAG CAG-3';
hs GAPDH forward 5'-GAG TCA ACG GAT TTG GTC GT-3';
hs GAPDH reverse 5'-GAC AAG CTT CCC GTT CTC AG-3';
mm Gapdh forward 5'-GTC ATC CCA GAG CTG AAC G-3';
mm Gapdh reverse 5'-TCA TAC TTG GCA GGT TTC TCC-3';
hs EMD forward 5'-CAT GAG GGT CTG GGC TTC AG-3';
hs EMD reverse 5'-GCA AGC ACT ACT CTG GGC TA-3';
hs TMPO LAP2B forward 5'-CCT CCT GCC TGT AGT GTG TG-3';
hs TMPO LAP2B reverse 5'-CGG ACA CAA AAG ACC CCA GA-3';
hs LEMD3 MAN1 forward 5'-GCC AAT CAT ACG GGC TCC AA-3';
hs LEMD3 MAN1 reverse 5'-GGG CAC TGA AAC TCC CTG TT-3';
hs TNFA forward 5'-GCC CCC AGA GGG AAG AGT TCC CCA-3';
hs TNFA reverse 5'-GCT TGA GGG TTT GCT ACA ACA TGG GC-3';
hs IL6 forward 5'-CCC CTG ACC CAA CCA CAA AT-3';
hs IL6 reverse 5'-ATT TGC CGA AGA GCC CTC AG-3';
hs IL1B forward 5'-CCA CCT CCA GGG ACA GGA TA-3';
hs IL1B reverse 5'-AAC ACG CAG GAC AGG TAC AG-3';
hs HMGN5 forward 5'-TCT GCC AGG TTG TCT GCT ATG-3';
hs HMGN5 reverse 5'-CAA CTG CTT GGG CAC TTG TAT-3';

cGAMP ELISA

For 2'3'-cGAMP quantification, cells were harvested by trypsination [Trypsin-EDTA (0.05%), Life Technologies] for 5 min. Cell pellets were lysed in RIPA lysis buffer containing 50 mM Tris, 150 mM NaCl, 1% (w/v) sodium deoxycholate, 0.03% (v/v) SDS, 0.005% (v/v) Triton X-100, 5 mM EDTA, 2 mM sodium orthovanadate, and cOmplete™ Protease Inhibitor Cocktail (Roche) (pellet from one well of a six-well plate in 130 µl of RIPA lysis buffer) for 30 min on ice. Lysed cells were centrifuged for 10 min at 18,200*g* and 4°C. The supernatant (100 µl) was used for the cGAMP ELISA assay (Cayman 2'3'-cGAMP ELISA kit, 501700) according to the manufacturer's instructions. Protein concentration in the supernatant was measured using BCA Pierce Protein assay kit and was used to normalize 2'3'-cGAMP levels.

Immunoblots

Cell pellets were lysed in RIPA lysis buffer containing 50 mM Tris, 150 mM NaCl, 1% (w/v) sodium deoxycholate, 0.03% (v/v) SDS, 0.005% (v/v) Triton X-100, 5 mM EDTA, 2 mM sodium orthovanadate, and cOmplete™ Protease Inhibitor Cocktail

(Roche). Protein concentration was measured using the BCA Pierce Protein assay kit and normalized to the lowest concentration. Protein extracts were diluted with loading buffer [100 mM Tris HCl (pH 6.8), 10% (v/v) SDS, 20% (v/v) glycerol, bromophenol blue, and 4% β-mercaptoethanol] and separated on SDS–PAGE [4-20% (Mini-PROTEAN® TGX™, Bio-Rad), 10% or 15% (v/v)] gels. Gels were transferred onto PVDF membranes (Immobilon-P) using the Trans-Blot® Turbo™ Transfer System (Bio-Rad). Membranes were briefly washed in Tris-buffered saline-Tween (TBS-T) [50 mM Tris-Cl pH 7.5, 150 mM NaCl, and 0.1% (v/v) Tween 20] followed by blocking in 5% non-fat dry milk (NFDM, Roth) TBS-T for 1 hour at room temperature. Primary antibodies were incubated in TBS-T 1% NFDM overnight at 4°C. Secondary antibodies were incubated in TBS-T 0.1% NFDM for 1 hour at room temperature. Proteins were visualized with the enhanced chemiluminescence substrate ECL (Pierce, Thermo Scientific) and imaged using the ChemiDoc XRS Biorad Imager and Image Lab 6.0.0 software. Imaging was performed in two channels: chemiluminescence and colorimetry.

Antibodies

Primary antibodies: anti-phospho-TBK1/NAK (Ser172) (clone D52C2) Rabbit mAb [immunoblot (IB): 1:500]; anti-TBK1/NAK (clone D1B4) Rabbit mAb (IB: 1:1000); anti-cGAS (clone D1D3G) Rabbit mAb [IB: 1:1000, immunofluorescence (IF): 1:200]; and anti-LaminA/C (clone 4C11), Mouse mAb (IF: 1:400) were purchased from Cell Signaling. Anti-β-Actin (clone C4), sc-47778, Mouse mAb (IB: 0.04 ng/µl final concentration); and anti-BAF (clone A11), s-166324, Mouse mAb (IB: 0.4 ng/µl and IF: 2 ng/µl final concentration), were purchased from Santa Cruz Biotechnology. Secondary antibodies: goat anti-Mouse IgG (H+L) Alexa Fluor® 488 conjugated (A-11001), goat anti-Rabbit IgG (H+L) Alexa Fluor® 488 conjugate (A-11008), donkey anti-Mouse IgG (H+L) Alexa Fluor 568 (A-10037) and goat anti-Rabbit IgG (H+L) Alexa Fluor 568 (A-11011) were purchased from Life Technologies. Secondary antibodies donkey anti-Rabbit HRP (711-036-152, IB: 1:2000) and donkey anti-Mouse HRP (715-036-151, IB: 1:5000) were purchased from Jackson ImmunoResearch.

Immunofluorescence

Cells were seeded onto coverslips at a density of 15,000 – 20,000 cells per coverslip and fixed with 4% (v/v) paraformaldehyde in PBS for 10 min, permeabilized for 5 min in 0.1% (v/v) Triton X-100 and blocked with 5% FBS (v/v) in PBS-T (0.1% Tween 20 in PBS) for 1 hour at room temperature. Cells were incubated with the primary antibody in PBS-T containing 5% FBS (v/v) for 16 hours at 4°C in a humid chamber. After washing with PBS-T, cells were incubated with the secondary antibody in PBS-T containing 5% FBS (v/v) for 1 hour at room temperature. Cells were washed with PBS-T and incubated with 1 µg/ml 4',6-diamino-2-phenylindole (DAPI) in PBS for 1 min at room temperature. Coverslips were mounted with Fluoromount-G (Southern Biotech).

For quantification of cGAS inside the nucleus, HeLa cells stained for cGAS and DNA were imaged using a Zeiss Axioplan 2 equipped with a 20X objective, 0.75 N.A, and an AxioCam MRm (CCD) camera. Images were analyzed using Fiji and its Cell Counter plugin. The ratio between normal nuclei and nuclei positive for cGAS was plotted using GraphPad Prism 8.

For quantification of cells with disrupted nuclei, HeLa cells stained for lamin A and DNA by DAPI were imaged using a laser scanning confocal microscope (Zeiss LSM700) equipped with a 20X objective, 0.80 N.A., using regular photomultiplier tubes (PMTs). Images were analyzed using Fiji and its Cell Counter plugin: Cells were enumerated by DAPI staining. Nuclear disruption was then assessed by lamin A staining. The percentage of cells harboring disrupted nuclei was plotted using GraphPad Prism 8.

To measure the NLS-GFP nucleus/cytosolic ratio, HeLa NLS-GFP stained for cGAS and DNA were imaged using a Zeiss Axioplan 2 equipped with a 63X oil immersion objective, 1.40 N.A., and an AxioCam MRm (CCD) camera. Using Fiji software, cells were split in two groups: positive (inside) or negative (outside) for cGAS within the nucleus. Each cell was then analyzed for NLS-GFP fluorescence intensity in and surrounding its nucleus with Cell Profiler 3.0.0. The ratio of NLS-GFP fluorescence inside/outside nucleus was then plotted using GraphPad Prism 8. Z-stacks were then analyzed using Imaris software (Bitplane). We defined a threshold for the green fluorescence channel to obtain a volume for cGAS binding onto DNA. Volumes were then plotted in Prism 8.0.

To measure the volume of cGAS binding inside the nucleus, HeLa cells treated with siBAF or siLMNA were stained for cGAS as described previously. DNA was stained with DRAQ5™ (5 µM, Thermo Fisher Scientific, 62252) for high-resolution microscopy. Z-stacks of cGAS binding to nuclear DNA were obtained using a high-resolution laser scanning confocal (Zeiss LSM710) microscope equipped with a 63X objective, 1.40 N.A., and 2-channel high-sensitivity BiG detectors to achieve 0.130-µm voxel depth. Z-stacks were analyzed using Imaris software (Bitplane). We defined a threshold for the green fluorescence channel to obtain a volume for cGAS binding onto DNA. Volumes were plotted using GraphPad Prism 8. To quantify micronuclei, HeLa cells treated with siBAF or siControl and stained for DNA by DAPI were imaged using a Zeiss Axioplan 2 with a 20X objective, 0.75 N.A., and an AxioCam MRm (CCD) camera. Quantification of micronuclei in cells was assessed using DAPI staining in Cell profiler. The ratio of micronuclei per cell was then plotted using GraphPad Prism 9.

To determine BAF and cGAS fluorescence intensity on transfected plasmid DNA, plasmid DNA was stained with DRAQ5™ for 10 min at room temperature before being transfected. HeLa cells overexpressing or not *BAF* and transfected with labeled plasmid DNA were stained for BAF and cGAS as described previously. Images were acquired using a laser scanning confocal microscope (Zeiss LSM700) equipped with a 20X objective, 0.80 N.A. using regular PMTs. Transfected plasmid was localized using DRAQ5™ staining and cGAS and/or BAF positivity in Cell Profiler 3.0.0 software. Intensity of both BAF and cGAS on transfected plasmid DNA were plotted using GraphPad Prism 9.

To visualize IRF3-GFP translocation upon cell confinement, compressed HeLa cells overexpressing *cGAS-Halo* and *IRF3-GFP* pre-treated with Blebbistatin (20 µM; (S)-4'-nitro-Blebbistatin, Cayman 24171) and siRNAs (see transfection protocol above) were fixed with PBS-PFA 4%, 5 hours after the 3-µm confinement. Fixed cells were stored in PBS. Images were acquired using a laser scanning confocal microscope (Zeiss LSM700) equipped with a 20X objective, 0.80 N.A., using regular PMTs. IRF3-GFP translocation was determined manually in cGAS-positive nuclei and plotted using GraphPad Prism 9.

Live-cell imaging

HeLa cells were plated into Falcon 96-well microplates [black; clear flat-bottom; TC-treated (Corning, 353219)] at a density of 7,500 cells per well. All live-cell imaging was performed using a Perkin Elmer Operetta CLS microscope equipped with a 20X objective, 0.80 N.A., and an Andor Zyla 5.5 (CMOS) camera at 37°C and under 5% CO_2. Lasers were used at 4–5% power.

For the quantification of nuclear envelope ruptures, HeLa NLS-GFP cells were treated with siRNA six hours after plating (see transfection protocol above). After one day of incubation and 1 hour prior to starting live imaging, cells were rinsed with PBS, incubated in DMEM fluorobrite (FluoroBrite™, Gibco, A1896701) supplemented with 10% (v/v) FCS, 1% (v/v) penicillin (100 IU/ml)/streptomycin (100 µg/ml), and 2 mM L-glutamine (complete media). To stain the nucleus, Hoechst 33342 (100 ng/ml) was added to the medium. For drug treatment, 1 hour prior to starting live imaging, cells were treated with 20 µM Blebbistatin ((S)-4'-nitro-Blebbistatin, Cayman 24171). Image acquisition was set to one picture every 5 min for 14 hours. Images were analyzed using Harmony® software (Perkin Elmer). For NLS-GFP analysis, cell nuclei were tracked using the Hoechst channel and the GFP intensity was measured inside tracked nuclei. GFP intensity data were extracted and submitted to analysis using R software. Briefly, we selected nuclei that were within the field for more than 100 frames (>8 hours 20 min) and followed their GFP fluorescence levels over time. Using the *findpeaks* function of R allowed for detection and analysis of a sudden decrease in GFP fluorescence. Identified peaks were only recorded if GFP recovery fitted to an exponential curve (r_squared = 0.90) with 35-min recovery.

Analysis of nuclear envelope rupture events was performed using HeLa *NLS-GFP cGAS-Halo* overexpressing cells transfected one day prior with an siRNA targeting *BAF*. Cells were treated with 100 nM cell-permeable HaloTag® TMRdirect ligand (Promega) in DMEM fluorobrite complete medium at 37°C and under 5% CO_2 for 1 hour prior to live imaging. Image acquisition was set to one picture every 5 min for 14 hours. Harmony® software (Perkin Elmer) was used to analyze the images. Monitoring NLS-GFP leakage was used to determine NE rupture events.

Fluorescence recovery after photobleaching (FRAP)

HeLa cGAS-GFP cells were plated on 35-mm glass bottom culture dishes (MatTek Corporation – Part Number P35G-1.5-14-C) at 5,000 cells per dish. Six hours later, cells were transfected with siRNA (see transfection protocol above). After 24 hours, cells were used for FRAP experiments, which were performed on a high-resolution laser scanning confocal (Zeiss LSM710) microscope at 37°C with a W-Plan Apochromat 63X water immersion objective, 1.0 N.A, using regular PMTs. A circle of 1.33-µm diameter (10 pixels) within cGAS-GFP particles located inside nucleus was partially photobleached with a 488-nm laser (100% power) with 10 iterations within 0.200 s. Time-lapse images were acquired over a 20-s time course after photobleaching with 0.200-s intervals with a laser power between 0.2% and 0.6%. Images were processed by Fiji and normalized on FRAP Analyser (software developed at the University of Luxembourg) using the Single Normalization+Full scale method. FRAP data were fitted to a binding+diffusion circular model using the FRAP Analyser. Immobile fraction extracted data were plotted in GraphPad Prism 8.

Cell cycle arrest

HeLa cells were treated with 2 mM thymidine (Sigma) twice per day during the course of the experiment. Transfection with respective siRNAs was performed 8 hours after the first treatment (see transfection protocol above), and cells were collected 72 hours after transfection.

Drug treatment

Cells were seeded into six-well plates to about 80% confluency. After 6 hours, doxycycline (1 μg/ml) and Valproic acid (VA, Sigma, 1 μM final concentration), Trichostatin A (TSA, Lucerna-Chem AG, 0.05 μM final concentration), or (S)-4'-nitro-Blebbistatin (Blebbistatin, Cayman 24171, 20 μM final concentration) were added. The medium was changed every 24 hours to replenish drugs and doxycycline. Samples were collected 72 hours after the onset of treatment.

Design and fabrication of the cell confinement device

The confinement device was manufactured using a protocol based on a previous publication (*18*). The polydimethylsiloxane (PDMS) (Dow Corning, Sylgard 184) device consists of three major components; a ring-shaped slab serving as a fixed boundary, a pneumatically-controlled piston moving in the center along the vertical axis, and a confinement module with microfabricated pillars that is attached to the bottom surface of the piston. The pillars define the geometry of the confinement during operation under vacuum. The outer PDMS ring fits on the plastic part of 35-mm glass-bottom petri dishes (MatTek, P35G-1.5-14-C) while the piston applies compression to the cells cultured on the cover slip. We set the height of the micropillars to 3 μm for effective rupture of the nucleus without initiating cell death.

Two stainless steel custom-made rings served as molds. The space between the outer and inner rings form a suction cup for the actuation of the piston. The rings were co-centered on a salinized [Sigma, Trichloro(1*H*,1*H*,2*H*,2*H*-perfluorooctyl) silane] silicon wafer and a 1:10 (curing agent:elastomer) ratio PDMS solution was poured on the mold. The devices were baked for an hour on a hot plate by gradually increasing the temperature to 95°C. After removing the devices from the mold, they were baked for another 10 hours at 65°C to complete the curing process. The mold for the micropillars was fabricated using dry etching. Briefly, positive photoresist (MicroChemicals, AZ1512) was spin-coated (Süss, ACS 200 Gen3) on a 102-mm silicon wafer, exposed to UV light with a mask aligner (Süss, MJB4), and etched (Alcatel AMS 200 SE) after development step (Süss, ACS 200 Gen3). The removal of the photoresist in acetone was accompanied with plasma stripping (PVA TePla 300) at 500 W for 5 min. Height measurements were performed using a mechanical profiler (Bruker, Dektak XT), which confirmed that the holes inside the molds were 3.1 ± 0.1 μm deep. A drop of 1:8 ratio PDMS solution was added on the silanized mold and a 1-mm round coverslip that had been activated with plasma cleaner (Plasma Harrick, PDC-002-HPCE) at 29 W for 2 min was pressed on the drop. After baking overnight at 65°C, the coverslips were peeled off the silicon wafer. The free glass surface of the coverslip and the bottom part of the PDMS piston were activated with O_2 plasma for 1 min to bond them with each other. Finally, a hole was generated on the outer wall using a biopsy puncher (Elveflow, 1.25-mm biopsy puncher) for the insertion of tubing that would apply vacuum during operation.

Operation of the cell confinement device

The pressure inside the suction cup was controlled using a precision vacuum generator system (AF 1 Dual VAN and AF 1 Dual, Elveflow). We set the vacuum at −10 mbar in the beginning of experiments while performing the alignment and attachment of the device to the petri dish. The applied vacuum was gentle enough to maintain the device on the culture dish without compressing the cells. We then applied lower values of pressure down to −100 mbar to move the piston down and squeeze the cells. The pillars ensure 3 μm confinement during long-term experiments. The confinement was released by slowly increasing the pressure back to −10 mbar. Images were taken using a motorized inverted fluorescence microscope (Nikon Eclipse Ti) at 10X or 20X magnification (Nikon) under physiological conditions. For time-lapse imaging, cells were maintained at 37°C and 5% CO_2 and the acquisition of images was automated using NIS-Elements software. After confinement, cells were left to recover 5 hours in an incubator (37°C and 5% CO_2) and were fixed for staining (see above), or their RNA content was extracted for analysis.

Expression and purification of recombinant human cGAS

Truncated human cGAS (155-522) was expressed and purified from *Escherichia coli (E.coli)* strain BL21 (DE3). Plasmids expressing His6-Halo tagged truncated human cGAS was induced with 2 mM IPTG at 18°C for 20 hours. Bacteria were collected by centrifugation and lysed by sonication in lysis buffer (20 mM HEPES, pH 8.0, 300 mM NaCl, 20 mM imidazole, 1 mM DTT, and protease inhibitor). After centrifugation, clear lysate was incubated with Ni-NTA beads (Qiagen), washed with lysis buffer, and with buffer containing 20 mM HEPES, pH 8.0, 1 M NaCl, 20 mM imidazole, and 1 mM DTT, and then eluted with 20 mM HEPES, pH 7.5, 500 mM NaCl, and 250 mM imidazole. Eluted cGAS was subjected to size-exclusion chromatography using a Superdex 200 16/60 column in 20 mM HEPES pH 7.5, 300 mM KCl and 1 mM DTT.

Expression and purification of recombinant human BAF

Plasmid expressing His6-MBP tagged BAF were transformed into BL21 (DE3) pLys *E.coli*. Cells were induced with 2 mM IPTG at 18°C for 20 hours. Bacteria were collected by centrifugation and lysed by sonication in 25 mM HEPES pH 7.5, 150 mM NaCl and protease inhibitor. Cell lysate was centrifuged for 30 min at 12,000*g* and the supernatant was discarded. The pellet fraction containing the His6-MBP tagged BAF was solubilized in buffer (25 mM HEPES pH 7.5, 150 mM NaCl, 25mM imidazole) containing 6 M guanidinium chloride and kept under agitation for 1 hour at 4°C. After centrifugation, clear lysate was incubated with Ni-NTA beads (Qiagen), washed extensively with solubilization buffer and eluted with 20 mM KH_2PO_4, pH 7.4, 0.5 mM EDTA, 10% glycerol, and 0.01% NP-40 complemented with 300 mM KCl, and 250 mM imidazole. The His6-MBP tag was cleaved by TEV protease at 37°C for 4 hours and dialysed overnight against 20 mM KH_2PO_4, pH 7.4, 0.5 mM EDTA, 10% glycerol, and 0.01% NP-40 complemented with 300 mM KCl. Cleaved protein was applied to Ni-NTA beads and the flow-through was collected. β-mercaptoethanol and EDTA were added to 50 mM and 10 mM respectively and the protein was incubated at room temperature for 30 min. BAF was refolded by extensive dialysis against 50 mM KH_2PO_4, pH 6.5, 200 mM NaCl, 10% glycerol, 10 mM EDTA and 50 mM β-mercaptoethanol.

BAF/cGAS in vitro competition assay

Full-length human cGAS (1 μM) or 20-to-1-equivalent recombinant human BAF were pre-incubated 1 hour with 0.1 mg/ml HT-DNA in Tris HCl 20 mM pH 8.0, and $MgCl_2$ 20 mM. Recombinant human BAF or cGAS respectively, 10 μCi [α-^{32}P]ATP and 1 mM GTP were added and left to react for 12 hours at 37°C. Reaction solution was spotted onto TLC plates (HPTLC silica gel, 60 Å pores, F_{254}, 1055480001; Merck Millipore), and the nucleotides were separated with 5 mM NH_4Cl 15% / 85% EtOH as the mobile phase at 25°C for 30 min. The plates were visualized by autoradiography. Images were processed using ImageLab (BioRad).

cGAS labeling

One equivalent Halo-tagged cGAS was incubated for 16 hours at room temperature with 1.1 equivalent Janelia Fluor 549 HaloTag ligand (Promega, GA1110). The labeled protein was purified using Zeba Spin desalting columns 7K MWCO (Thermo Fisher Scientific, 89882) according to the manufacturer's instructions.

cGAS ELISA

90mer-Biotin (5 pmol/well) was incubated for 1 hour in streptavidin-coated plates (Pierce, 15125). Recombinant human BAF WT or BAF G47E (10 μM to 1 μM) in PBS 1% BSA were incubated for 30 min at room temperature in the DNA-functionalized plate. Recombinant human cGAS 155-522 Halo-His (0.25 μM in PBS 1% BSA) was added and incubated 3 hours at room temperature. Wells were washed three times with PBS 1% BSA and 0.1% Tween 20. Bound recombinant cGAS was then detected using anti-His Tag antibodies (clone D3I10, Cell Signaling) and horseradish peroxidase-conjugated donkey anti-rabbit secondary antibody (Jackson Immunoresearch, 711-036-152).

cGAS preparation and labeling for single-molecule total internal reflection microscopy (smTIRF)

Truncated human cGAS (155-522)-Halo was expressed and purified as described above. For cGAS-Halo labeling, Janelia Fluor-549 HaloTag (Janelia, JF-549) was added at a protein-to-dye ratio of 1:1.1 followed by incubation for 1 hour. Labeled cGAS-Halo was finally purified by size exclusion chromatography (SEC) using a Superose6 10/300 GL column (GE healthcare) in 20 mM HEPES pH 7.5, 300 mM NaCl, 1 mM DTT buffer using a flow-rate of 0.4 ml/min. Fractions were analyzed using SDS–PAGE, clean fractions were pooled and protein concentration was determined using UV spectrophotometry (at A_{280} and A_{571}). Finally, labeling efficiency was calculated by using the extinction coefficients for cGAS-Halo (99,070 mol^{-1} cm^{-1}) and JF-549 (101,000 mol^{-1} cm^{-1}). Typical labeling efficiency was found to be >90%.

DNA preparation and labeling for smTIRF

dsDNA (230 bp) containing one copy of Widom 601 DNA nucleosome positioning sequence (*27*) was produced by PCR with forward biotinylated primer 5'-Biotin-CGCACACT-(amine-linker)-GTGCCAAGTACTTAC-3' (Integrated DNA Technologies) labeled with Alexa Fluor 647 NHS ester (Life Technologies) according to

the manufacturer's protocol (Life Technologies) and 5'-ATCCGGAGTACTTGGTCTC-3' reverse primer (Integrated DNA Technologies). The excess of the primers was removed by purification with QIAquick PCR purification kit (Qiagen), and the final product was purified by ethanol precipitation.

smTIRF experiment

Measurements were performed as described previously (*29*). Briefly, objective-type smTIRF was performed using a Nikon Ti-E inverted fluorescence microscope, equipped with a CFI Apo TIRF 100X oil immersion objective, N.A. 1.49, an ANDOR iXon EMCCD camera and a TIRF illuminator arm. Laser excitation was realized using a Coherent OBIS 640LX laser (640 nm, 40 mW) and coherent OBIS 532LS laser (532 nm, 50 mW). For all smTIRF experiments, flow channels were prepared as described before (*29*) washed with 500 µl degassed ultrapure water (Romil), followed by 500 µl of 1X T50 (10 mM Tris pH 8.0, and 50 mM NaCl) and background fluorescence was recorded with both 532 nm and 640 nm excitation. 50 µl of 0.2 mg/ml neutravidin was then injected and incubated for 5 min, and washed using 500 µl 1X T50. Alexa 647 labeled DNA (100 pM) in 1X T50 with 2 mg/ml bovine serum albumin (BSA, Carl Roth) was flowed into the channel for immobilization. 500 µl 1X T50 was used to wash out unbound DNA. 1× T50 buffer was exchanged to the imaging buffer imaging buffer (50 mM HEPES pH 7.5, 100 mM NaCl, 0.05% v/v Tween 20, 2 mM Trolox, 3.2% w/v glucose, 1X glucose oxidase/catalase oxygen scavenging system, and 2 mg/ml BSA). JF-549-labeled cGAS-Halo (20 nM) was flowed in using imaging buffer and movies were recorded at 5 Hz in TIRF illumination, alternating between far-red and green illumination (1:200 frames). The same movies were recorded after injection of JF-549-labeled cGAS-Halo in presence of 500 nM unlabeled BAF WT or BAF G47E proteins.

Data analysis of smTIRF

Single-molecule trace extraction and trace analysis were performed as described in (*29*) with some adjustments. Movies were background-corrected using a rolling ball algorithm in ImageJ. DNA positions were detected using a custom built Matlab (Mathworks) script employing a local maxima approach. Images were aligned to compensate for stage drift. Fluorescence intensities (in the orange channel) were extracted within a 2-pixel radius of the identified DNA peaks. Individual detections were fitted with a 2D-Gaussian function to determine co-localization with immobilized DNA. Detections exceeding a PSF width of 400 nm, a 250 nm offset from the DNA position or an intensity >5000 counts were excluded from further analysis. Individual traces were analyzed by a step-finding algorithm (*28*), followed by thresholding. Overlapping multiple binding events were excluded from the analysis. For each movie cumulative histograms were constructed from detected bright times (t_{bright}) corresponding to bound cGAS molecules to obtain dwell-times and dark times (t_{dark}) to obtain on-rate constants, usually including data from ~100 individual traces. The cumulative histograms from traces corresponding to individual DNA were fitted with diexponential functions.

Chromatin purification

Chromatin was purified from HeLa cells as previously described (*16*) with some modifications. Briefly, HeLa cells were harvested by trypsination and 10^7 cells were washed in PBS, resuspended in lysis buffer (20 mM Tris pH 7.5, 100 mM NaCl, 0.01% Triton X-100, 5 mM $MgCl_2$, and 0.2% NP-40 equivalent) on ice, and lysed by five strokes through a 0.4×19-mm needle. The lysate was centrifuged for 3 min at 3,400*g*, 4°C, then the pellet was resuspended in high salt buffer (20 mM Tris pH 7.5, 1 M NaCl, 0.01% Triton X-100, and 5 mM $MgCl_2$) and incubated for 5 min on ice, followed by centrifugation for 5 min at 18,200*g* at 4°C. The pellet was again resuspended in high salt buffer, incubated for 5 min on ice, and centrifuged for 5 min at 18,200*g*. Finally, the pellet was resuspended in storage buffer (20 mM Tris pH 7.5, 150 mM NaCl, 0.01% Triton X-100, and 10% glycerol). Chromatin was sheared by eight strokes through a 0.8×38 mm needle and snap-frozen.

Chromatin assay

Glass-bottom microwell dishes (MatTek, P35G-1.5-14-C) were coated with 100 µl of Poly-L-Lysine for 10 min at room temperature. Chromatin diluted in 100 µl buffer (Tris 20 mM pH 7.5, NaCl 150 mM, Triton X-100 0.01%, $MgCl_2$ 0.2 mM, DTT 1 µM, and Hoechst 33342 0.5 µg/ml) was deposited into coated wells and allowed to adhere for 10 min at room temperature. Purified human BAF recombinant protein (1, 2.5, or 10 pmol) was added to the chromatin and incubated for 10 min. Finally, purified human recombinant labeled-cGAS (15 pmol) was added in the dishes. Images were acquired by a laser scanning confocal microscope (Zeiss LSM700) equipped with a 20X objective, 0.80 N.A., using regular PMTs, and processed in Cell Profiler 3.0.0 software.

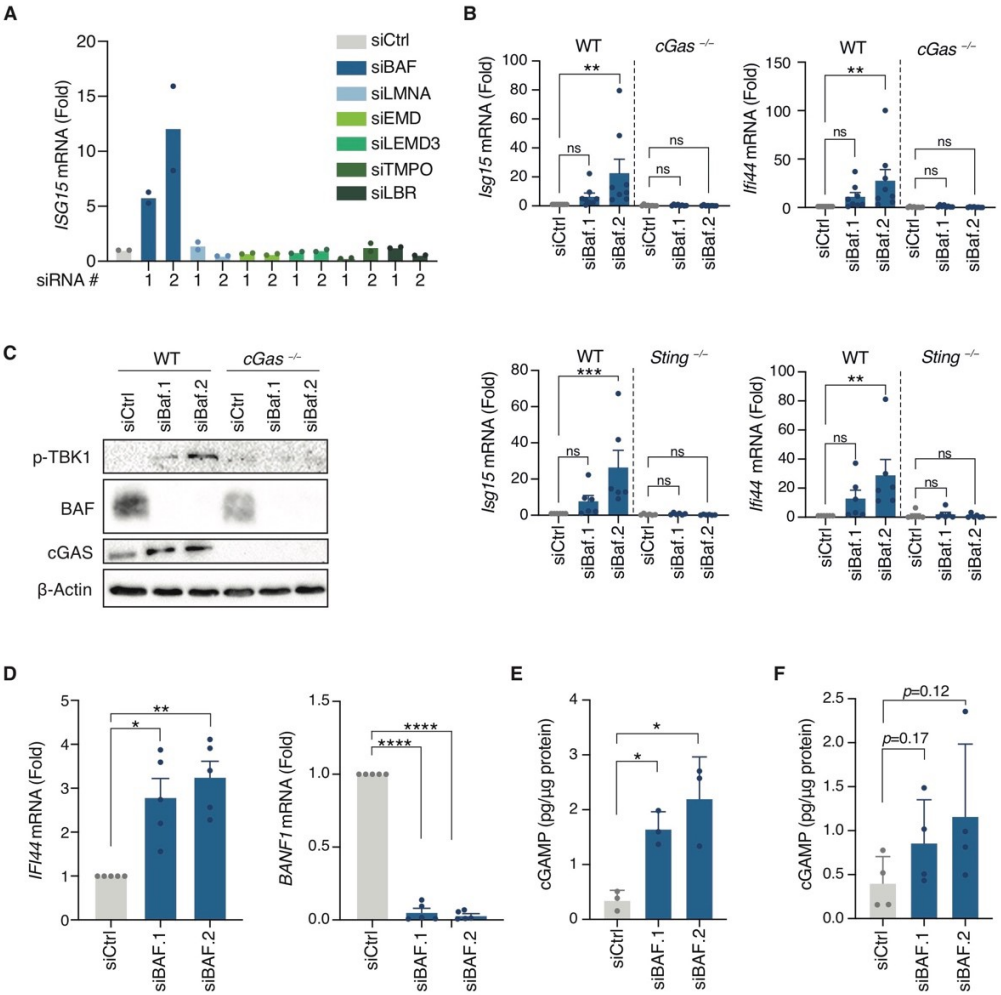

Fig. S1. Knockdown of *BAF* activates the cGAS–STING pathway.

(**A**) *ISG15* induction in HeLa cells treated with a control siRNA or siRNAs targeting genes involved in NE maintenance (N = 2). (**B**) ISG (*Isg15*, *Ifi44*) induction in WT, *cGas*$^{-/-}$ and *Sting*$^{-/-}$ MEFs treated with a control siRNA (siCtrl) or siRNAs against *BAF* (siBaf.1 and siBaf.2). (*cGas:* N = 8*, Sting:* N = 6). One-way ANOVA with post hoc Dunnett multiple comparison test. (**C**) Phosphorylation of TBK1 in WT and *cGas*$^{-/-}$ MEFs after *BAF* knockdown. (**D**) mRNA expression levels of *IFI44* and *BAF* in human WI-38 cells after treatment with siCtrl or siBAF.1 and siBAF.2 (N = 5). One-way ANOVA with post hoc Dunnett multiple comparison test. (**E** and **F**) 2'3'-cGAMP quantification in primary human adult dermal fibroblasts (**E**) and primary human neonatal foreskin fibroblasts (**F**) treated with a siCtrl or siBAF.1 and siBAF.2 (N = 3 and N = 4, respectively). One-way ANOVA with post hoc Dunnett multiple comparison test. Error bars, SEM. *P < 0.05; **P < 0.01; ***P < 0.001; ****P < 0.0001; ns, not significant.

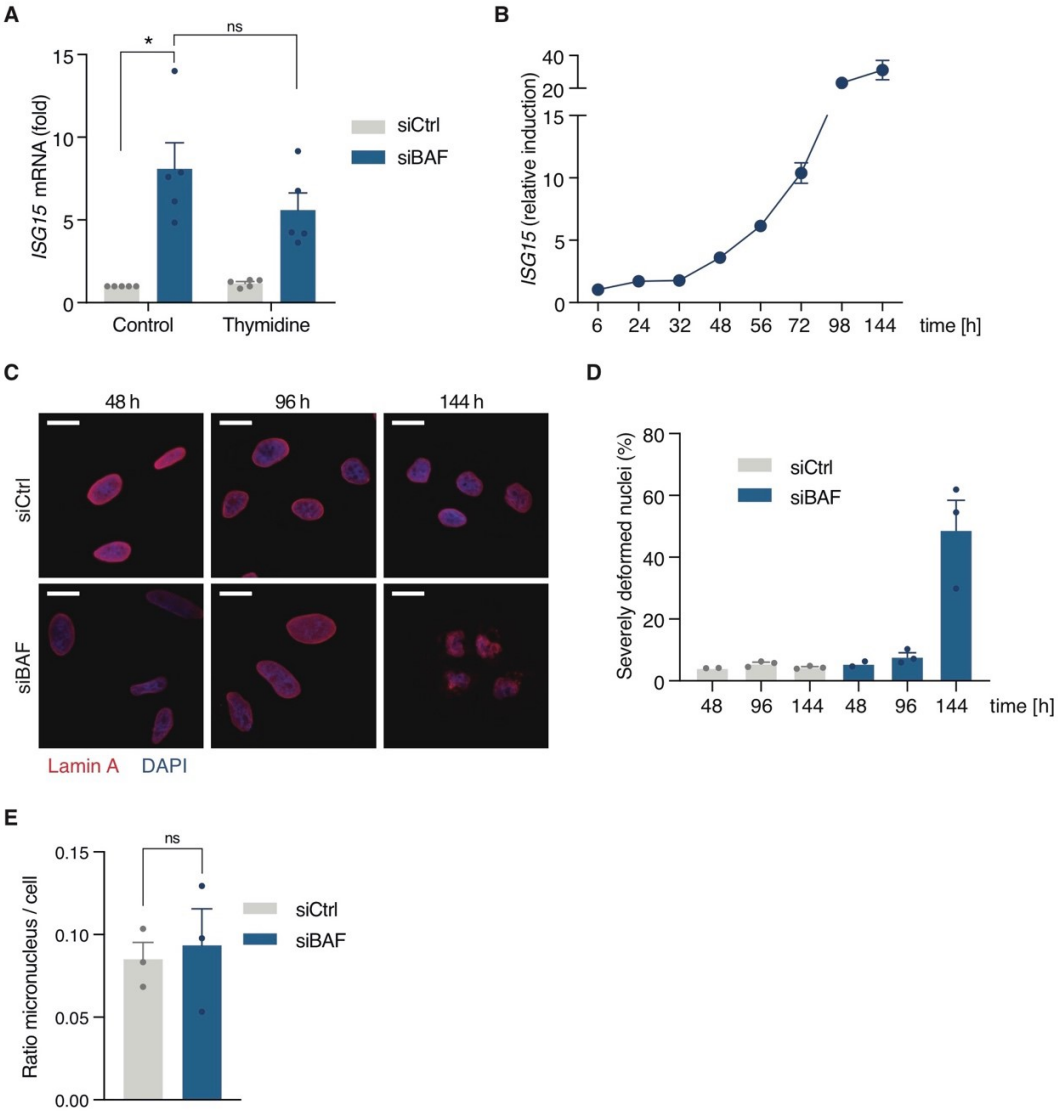

Fig. S2. ISG induction occurs independently of cell cycle arrest and nuclear fragmentation.

(**A**) *ISG15* induction in HeLa cells depleted or not for *BAF* (siBAF) and left untreated or arrested in S phase of the cell cycle through addition of thymidine (N = 5). One-way ANOVA with post hoc Tukey multiple comparison test. (**B**) Kinetics of *ISG15* induction in HeLa cells after knockdown of *BAF* (siBAF) in comparison to cells treated with control siRNA (N = 3). (**C** and **D**) Representative images and quantification of nuclear shape in HeLa cells after knockdown of *BAF* (siBAF) over time. Scale bar: 20 µm. DAPI, blue; lamin A, red (N = 2 (48 hours), N = 3 (96 hours and 144 hours). (**E**) Micronuclei quantification per cell by immunofluorescence in HeLa cells after *BAF* knockdown (siBAF) (N = 3). Error bars, SEM. *$P < 0.05$; ns, not significant.

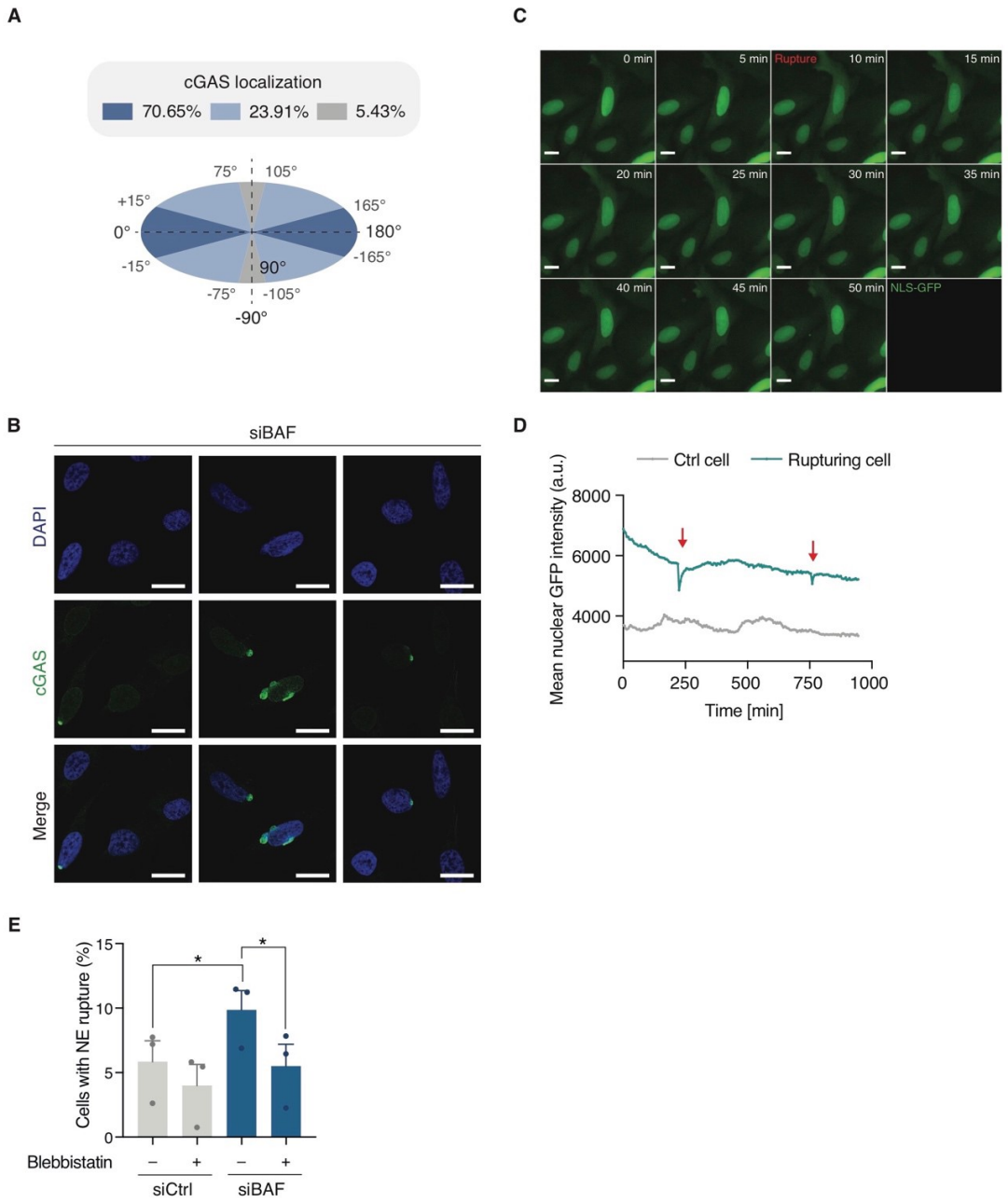

Fig. S3. cGAS accumulates inside ruptured nuclei upon *BAF* knockdown.

(**A**) Distribution pattern of translocated cGAS relative to the elliptical nucleus surface area. (**B**) Representative confocal fluorescence microscopy images of *BAF*-KD HeLa cells stained for cGAS (green). DAPI shown in blue. Scale bar: 20 µm. (**C**) Image sequence of a NE rupture in a *BAF*-KD HeLa cell expressing *NLS-GFP*. Scale bar: 20 µm. (**D**) Representative graph of a cell exhibiting a NE rupture event (green)

compared to a cell without *NLS-GFP* expression (gray). Shown is the mean fluorescence intensity in arbitrary units (a.u.) of nuclear GFP. Abrupt loss of fluorescence intensity marks a NE rupture event, highlighted by red arrows, which is followed by NLS-GFP reimport. (**E**) Incidence of NE rupture in the presence or absence of blebbistatin in HeLa cells treated with control siRNA (siCtrl) or siRNA against *BAF* (siBAF), (N = 3). One-way ANOVA with post hoc Tukey multiple comparison test. Error bars, SEM. $^{*}P < 0.0001$.

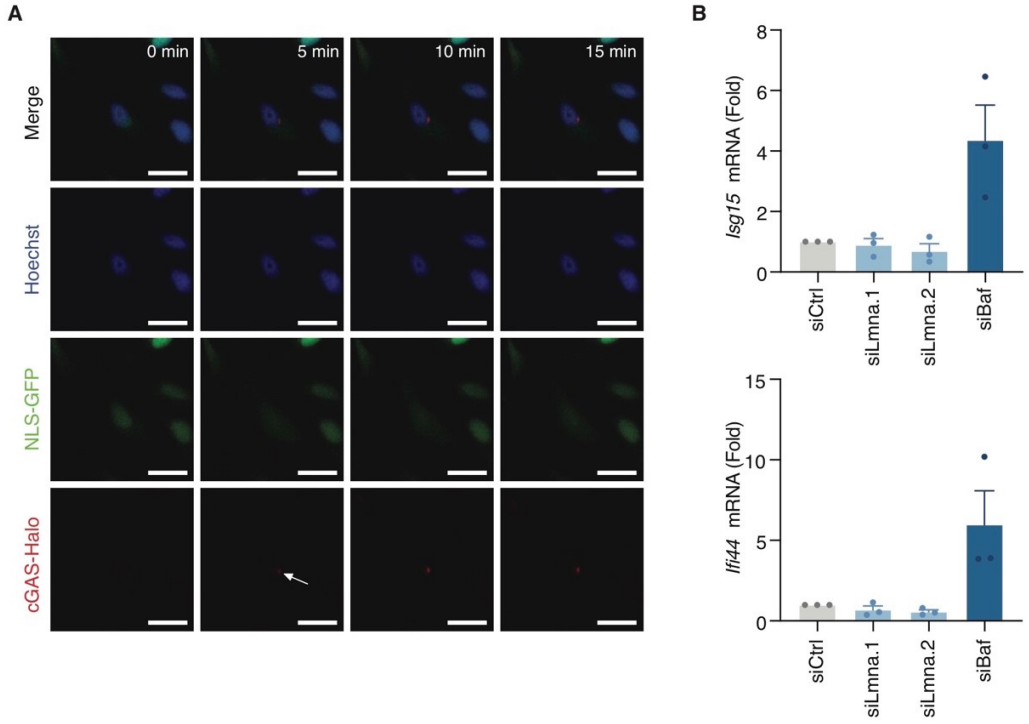

Fig. S4. Lamin A suppression induces NE rupture but not cGAS activation.

(**A**) Representative image sequence of a *LMNA*-depleted HeLa cell exhibiting a NE rupture event (escape of NLS-GFP (green)) accompanied by cGAS-Halo (orange) intranuclear accumulation. Arrow indicates cGAS entry into the nucleus. Scale bar: 50 µm. (**B**) MEFs were treated with siRNAs against *Lmna* (siLmna.1 and siLmna.2) or *Baf* (siBaf) and mRNA expression levels of *Isg15* and *Ifi44* were assessed relative to MEFs treated with a non-targeting control siRNA (N = 3). Error bars, SEM.

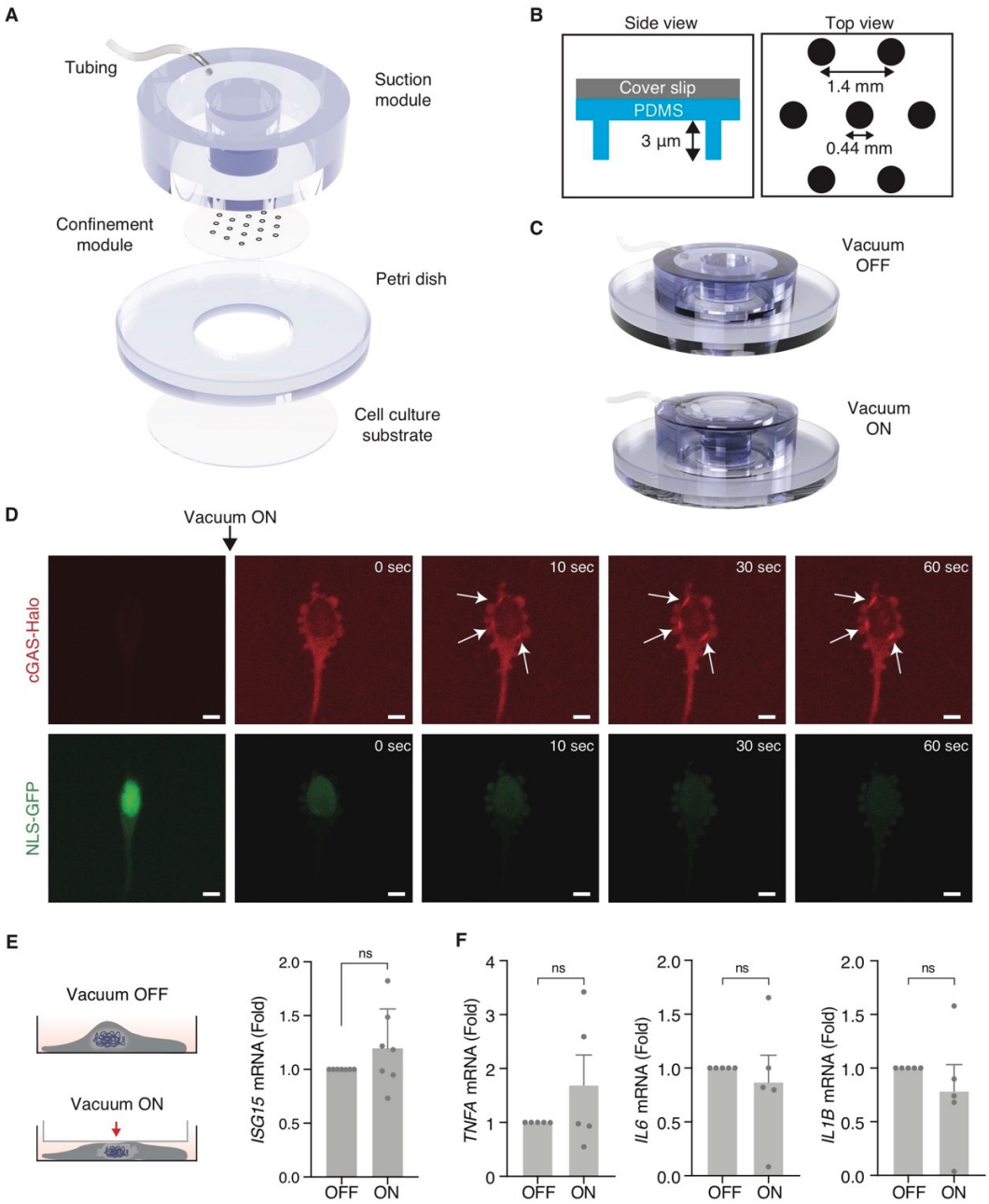

Fig. S5. Cell confinement studies.

(**A**) Exploded view of the confinement device. Cells are cultured on the cell culture substrate, which is glued onto the petri dish. The microfabricated confinement module was bonded onto the bottom of the piston. Upon vacuum through the tubing, the piston moves along the vertical axis and compresses the cells on the cell culture substrate. (**B**) Left: schematic side view of the confinement module, marking the confinement height (3 µm). Right: corresponding schematic top view of the confinement module. The pillars keep the height uniform throughout the confinement module. (**C**) Schematic 3D overview

of the whole device while vacuum off and on, respectively. Not to scale. (**D**) Representative image sequence of a HeLa cell under 3-μm confinement and expressing cGAS-Halo (red) and NLS-GFP (green). Arrows highlight cGAS accumulation on nuclear chromatin. Scale bar: 10 μm. (**E**) HeLa cells were kept under 3-μm confinement for 1 min and recovered overnight before assessing mRNA levels of *ISG15*. (N = 7). Student's t test. Error bars, SEM. ns, not significant. (**F**) HeLa cells were subjected to transient cell confinement and recovered overnight before assessing mRNA levels of proinflammatory genes (N = 5). Student's t test. Error bars, SEM. ns, not significant.

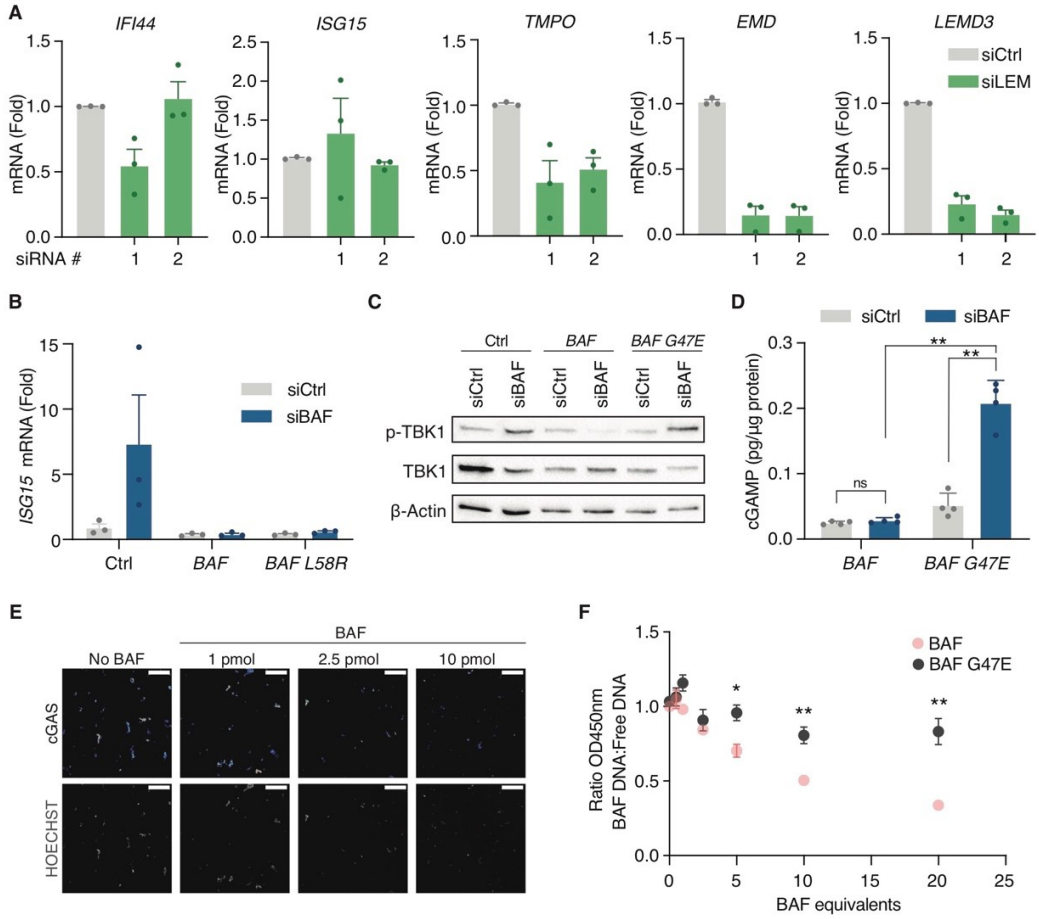

Fig. S6. Loss of dimerization, but not LEM interaction, regulates cGAS activity upon BAF dysfunction.

(**A**) mRNA expression levels of indicated genes in HeLa cells treated with a control siRNA (siCtrl) or siRNAs targeting simultaneously *TMPO*, *EMD*, and *LEMD3* (siLEM) (N = 3). (**C**) *ISG15* mRNA expression levels from HeLa cells (Ctrl) and siRNA-resistant *BAF (WT)* and *BAF L58R* expressing HeLa cells after knockdown of endogenous *BAF* (N = 3). (**D**) Phosphorylation of TBK1 in HeLa cells (Ctrl) and siRNA-resistant *BAF (WT)* and *BAF G47E* expressing HeLa cells after knockdown of endogenous *BAF*. Results are representative of three independent experiments. (**E**) 2'3'-cGAMP quantification in siRNA-resistant *BAF (WT)* and *BAF G47E* expressing HeLa cells after knockdown of endogenous *BAF* (N = 4). **(F)** Representative images of cell-derived chromatin incubated with purified human cGAS and increasing amounts of purified human BAF. Scale bar: 20 µm. (**G**) Ratio of cGAS binding to DNA pre-complexed with BAF WT or BAF G47E, and free DNA, (N = 3), multiple t test. Error bars, SEM. $^{**}P < 0.01$; ns, not significant.

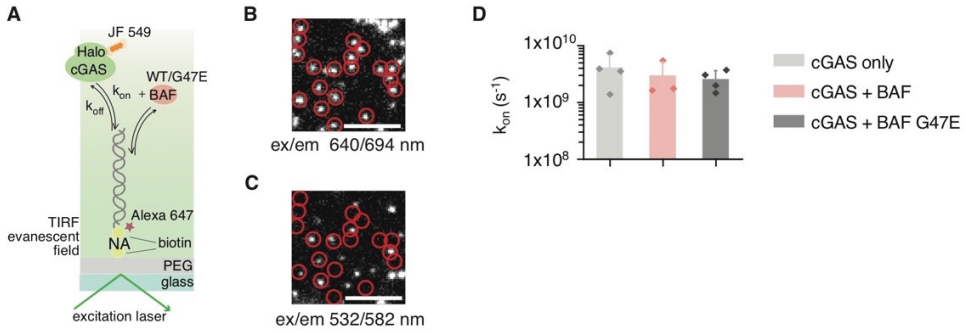

Fig. S7. Single-molecule imaging demonstrates that BAF displaces cGAS from dsDNA.

(**A**) Schematic of the single-molecule (sm) TIRF experiment: cGAS, labeled with JF-549, is injected into flow cells containing immobilized DNA, in the absence or presence of BAF WT or BAF G47E. Dynamic cGAS binding events are detected by colocalization of smTIRF images. (**B**) Detection of DNA localizations using smTIRF. (**C**) Single cGAS binding events are detected at DNA positions by smTIRF via a colocalization algorithm. Scale bars in (**B**) and (**C**): 5 µm. (**D**) On-rate constants obtained from histograms of t_{dark}.

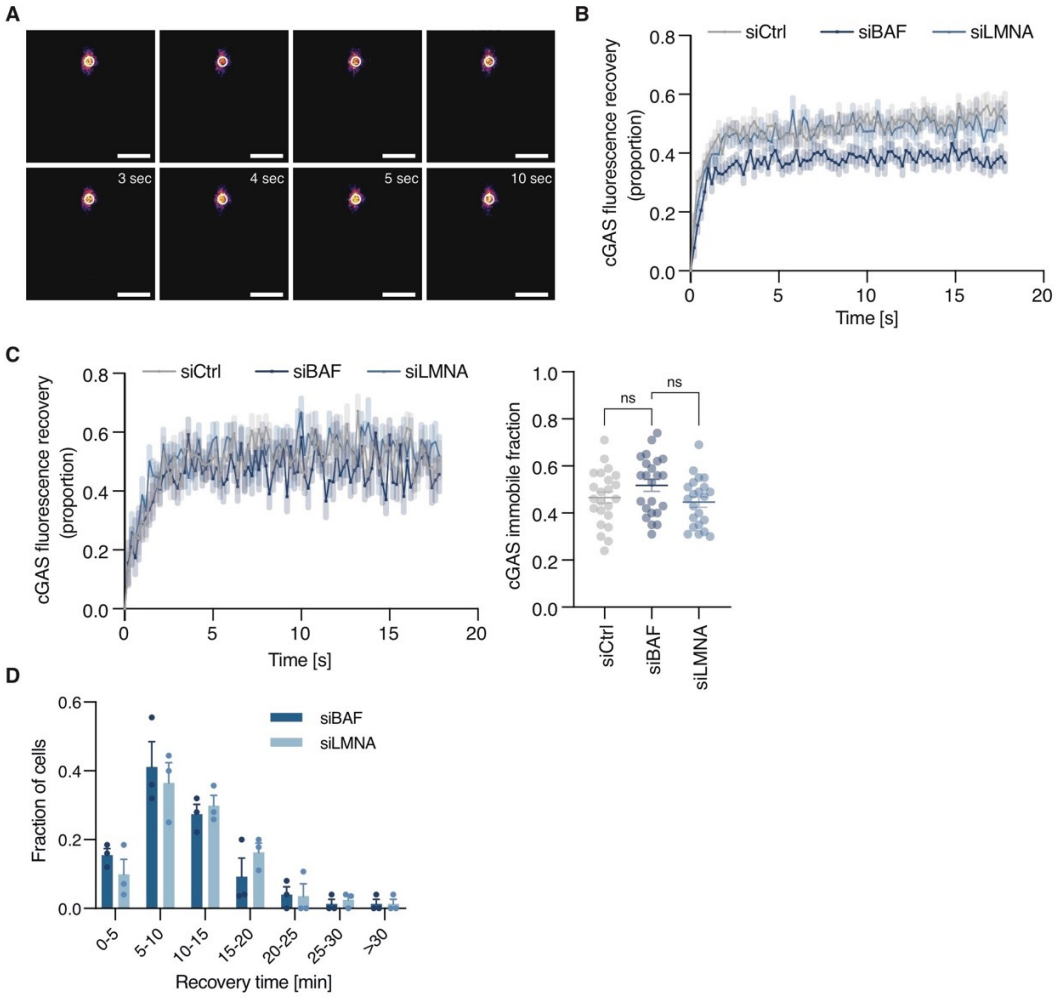

Fig. S8. NE rupture recovery and cGAS-Halo mobility in control cells, *BAF*-depleted or *LMNA*-depleted cells.

(**A**) Representative confocal fluorescence microscopy images of live HeLa cells expressing GFP-tagged cGAS after knockdown of *BAF*. Scale bar: 5 µm. (**B**) Line curves show FRAP of cGAS-GFP localized at the rupture site in HeLa cells treated with siCtrl, siBAF, or siLMNA. Data represent mean ± SEM from 16-20 measurements. Graph is representative of three independent experiments. (**C**) Left: Line curves show FRAP of cGAS-GFP localized within the nucleus of HeLa cells treated with siCtrl, siBAF, or siLMNA. Data represent mean ± SEM from 20-25 measurements. Graph is representative of three independent experiments. Right: cGAS-GFP immobile fraction obtained after photobleaching of nuclear cGAS-GFP in HeLa cells treated with siCtrl, siBAF, or siLMNA (representative of three independent experiments). **(D)** NLS-GFP fluorescence half-time recovery after NE rupture in HeLa cells treated with siRNAs targeting *BAF* (siBAF) or *LMNA* (siLMNA) ($N = 3$). One-way ANOVA with post hoc Dunnett multiple comparison test. Error bars, SEM. ns, not significant.

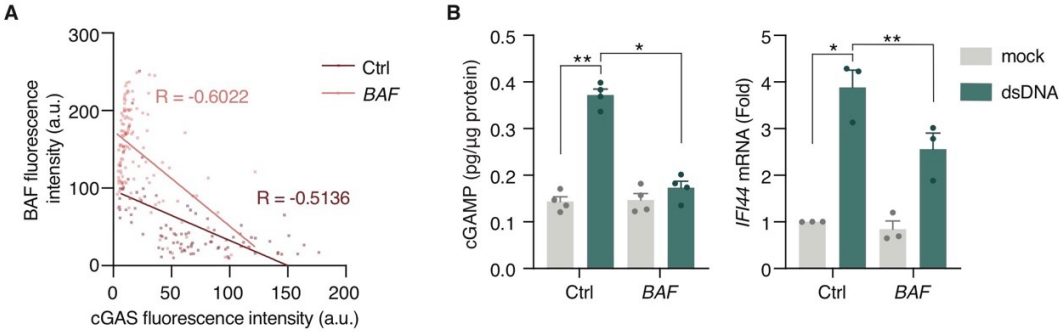

Fig. S9. Competition for DNA binding between cGAS and BAF in the cytoplasm.

(**A**) cGAS and BAF fluorescence intensity on transfected plasmid DNA. Each dot represents BAF/cGAS fluorescence on one single transfected plasmid particle (representative of three independent experiments). R correlation factor Pearson. (**B**) 2'3'-cGAMP levels (left) and *IFI44* induction (right) of HeLa cells overexpressing *BAF* (*WT)* or controls, and transfected or not with plasmid DNA (left panel: $N = 4$, right panel: $N = 3$). One-way ANOVA with post hoc Dunnett multiple comparison test. Error bars, SEM. $^{*}P < 0.05$; $^{**}P < 0.01$.

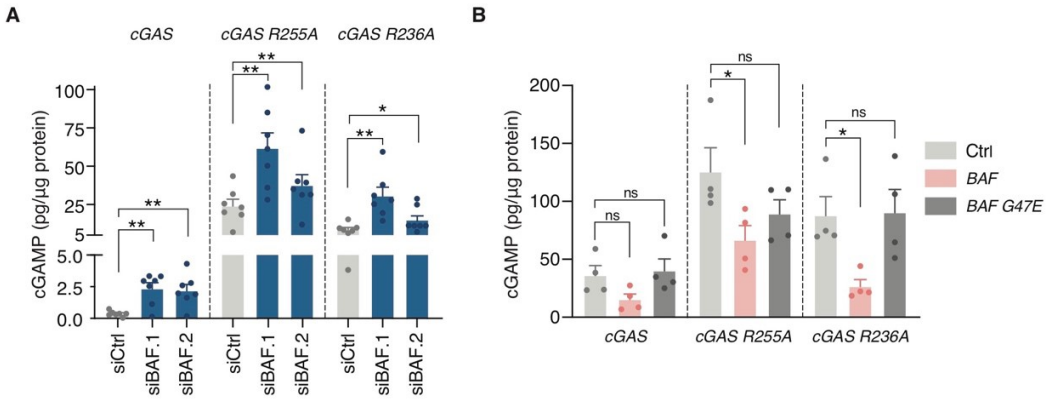

Fig. S10. BAF restricts cGAS activity independently of chromatin tethering.

(**A**) 2'3'-cGAMP quantification in *CGAS*$^{-/-}$ HeLa cells overexpressing *cGAS (WT)*, *cGAS R255A,* or *cGAS R236A* and treated with a control siRNA (siCtrl) or siRNAs against *BAF* (siBAF.1, siBAF.2) (N = 7). One-way ANOVA with post hoc Dunnett multiple comparison test. (**B**) 2'3'-cGAMP quantification in *CGAS*$^{-/-}$ HeLa cells overexpressing *cGAS (WT)*, *cGAS R255A,* or *cGAS R236A*, and transfected with a control plasmid (Ctrl) or one carrying *BAF* (WT) or *BAF G47E* (N = 4). One-way ANOVA with post hoc Dunnett multiple comparison test. Error bars, SEM. *P < 0.05; **P < 0.01; ns, not significant.

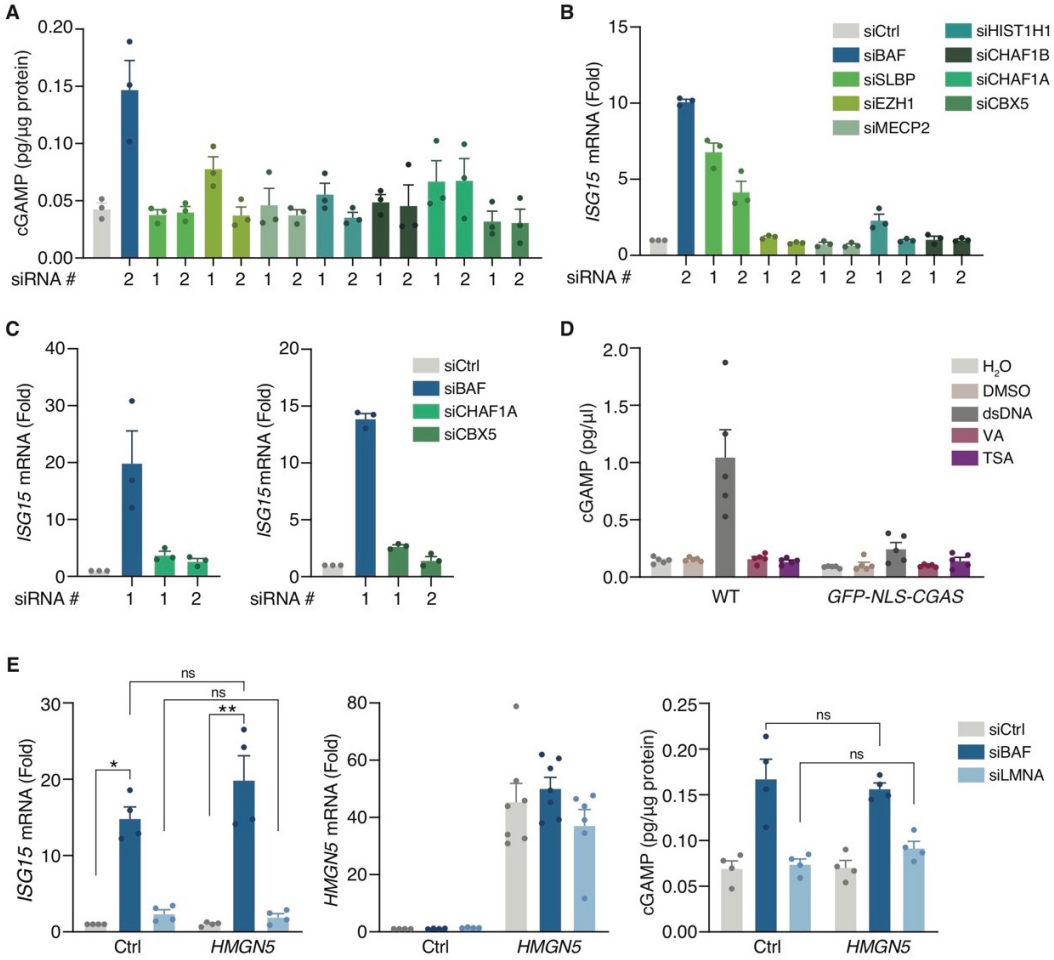

Fig. S11. Perturbation of chromatin architecture does not activate cGAS.

(**A**) 2'3'-cGAMP quantification in HeLa *CGAS*$^{-/-}$ cells overexpressing *GFP-NLS-cGAS* and treated with siRNAs targeting *BAF* (siBAF) or other architectural chromatin factors (siRNAs 1 and 2, respectively) as indicated (N = 3). (**B** and **C**) *ISG15* mRNA expression in HeLa cells after knockdown of *BAF* or other architectural chromatin factors (siRNAs 1 and 2, respectively) as indicated (N = 3). (**C**) 2'3'-cGAMP quantification in HeLa WT cells (WT) or HeLa *CGAS*$^{-/-}$ cells overexpressing *GFP-NLS-cGAS* treated with controls (H_2O or DMSO), valproic acid (VA), trichostatin A (TSA), or 90mer DNA (dsDNA) (N = 5). (**D**) mRNA expression levels of *ISG15* and *HMGN5* and 2'3'-cGAMP quantification in HeLa cells overexpressing *HMGN5* and treated with control siRNAs (siCtrl) or siRNAs targeting *BAF* (siBAF) or *LMNA* (siLMNA) (N = 4). One-way ANOVA with post hoc Dunnett multiple comparison test. Error bars, SEM. *P < 0.05; **P < 0.01; ns, not significant.

Movie S1. Nuclear envelope rupture upon *BAF* depletion (related to Fig. 1G).

Representative live-cell imaging of a *BAF*-depleted HeLa cell exhibiting a NE rupture event (NLS-GFP (green) escape) accompanied by cGAS-Halo (orange) intranuclear accumulation. Time-lapse images were acquired with 5-min intervals.

Movie S2. cGAS mobility on chromatin measured by FRAP (related to fig. S8A).

Representative confocal fluorescence microscopy image sequence of intranuclear photobleaching (at time point 00:02 min) of GFP-tagged cGAS and fluorescence recovery in a live HeLa cell after *BAF* knockdown. Time-lapse images were acquired over a 18-s time course after photobleaching with 0.200-s intervals.